DEVELOPMENT OF A FRANGIBLE DESIGN FOR A SMALL FIXED-WING UNMANNED AERIAL SYSTEM

A Thesis

by

ANURAG

Submitted to the Graduate and Professional School of
Texas A&M University
in partial fulfillment of the requirements for the degree of

MASTER OF SCIENCE

Chair of Committee,	Thomas E. Lacy Jr.
Committee Members,	Douglas Allaire
	Darren Hartl
	Kalyan Raj Kota
Head of Department,	Guillermo Aguilar

December 2022

Major Subject: Mechanical Engineering

ABSTRACT

Small (< 25 kg) fixed-wing unmanned aerial systems (UASs) impacts can cause severe damage to manned aircraft. At impact velocities of ∼128.6 m/s, small UASs can perforate aircraft skins and damage underlying load carrying structures (ribs, spars, *etc.*) which can hinder flight safety. Severe impact damage is primarily due to an in-line arrangement of relatively heavy and stiff UAS components, *i.e.,* motor, battery, and payload. In this work, a frangible design for a nominal 1.8 kg (4 lb) fixed-wing UAS was developed using finite element analysis to reduce the impact severity of airborne collisions to manned aircraft. The baseline UAS with a 'tractor' engine configuration (motor as the foremost part of the UAS) was modified to a 'pusher' engine configuration (motor in the aft of the fuselage) in developing the frangible design. A series of impacts were simulated in LS-DYNA with the pusher fixed-wing UAS configuration impacting a 1.59 mm thick aluminum 2024-T3 flat-plate target at 128.6 m/s to evaluate different frangible design concepts. A polymeric foam nosecone was introduced at the front of the UAS to absorb impact energy. Expanded polypropylene (EPP), polyurethane (PUR), and polystyrene based IMPAXX700 foams were assessed for the nosecone materials. Conical and semispherical nosecone geometries were considered for the preliminary analysis and subsequently, a topologically optimized nosecone geometry was designed for improved energy absorption. In addition, a payload drop mechanism was designed to initiate payload redirection from the in-line collision trajectory of the battery and motor. This minimized direct multi-component single-axis impacts on the target. These mechanisms reduced the target impact damage compared to the tractor configuration but were unsuccessful in avoiding the target plate tearing. Ultimately, crushable corrugated aluminum tubes positioned ahead of the payload within the fuselage and a crushable corrugated Al nosecone were designed to enhance impact energy absorption for the UAS which successfully avoided the target plate penetration and had a 39% safety margin based on the target plate strain-to-failure. This frangible UAS design will significantly reduce the impact damage to manned aircraft in airborne collision scenarios.

ACKNOWLEDGMENTS

First and foremost, I would like to express my sincere thanks to my advisor Dr. Thomas E. Lacy Jr. for providing me with this opportunity to pursue my masters on such a challenging topic and for his constant guidance and support throughout this journey. Dr. Lacy is an expert on Finite Element Analysis and is the one who ensured that I have strong foundation in Finite Element concepts and made it a great learning experience for me. He appreciated me, motivated me, and encouraged me through all the different phases of my thesis. Next, I would like to thank Dr. Raj Kota for his wise and stern mentorship where he always pushed me to do the best. He spent ample time in teaching me the intricacies of the tools that I used in my thesis and was always there to resolve my queries. He mentored me for my work and for my career as well. I have learned a lot from the discussions we had.

I am appreciative of Texas A&M University and Texas A&M High Performance Research Computing center for providing the resources and IT support without which this work would not have been possible.

Also, I would like to express my heartfelt gratitude for my parents Neeraj Kumar and Vandna Joshi and my brother Abhishek for their love, care, concern, encouragement, sacrifices, and blessings throughout my life. I would also like to thank my family, friends, and colleagues who supported and motivated me, and ensured that I always had smile on my face while I worked.

CONTRIBUTORS AND FUNDING SOURCES

Contributors

This work was supported by a thesis committee consisting of Professor Thomas E. Lacy - advisor and Associate Professor Douglas Allaire of the Department of Mechanical Engineering, Senior Research Engineer II Kalyan Raj Kota of TEES and Bush Combat Development Complex of Texas A&M University System, and Associate Professor Darren Hartl of the Department of Aerospace Engineering.

The UAS finite element model for the work was provided by Dr. Thomas E. Lacy and Dr. Kalyan Raj Kota and the target plate model was provided by National Institute for Aviation Research, Wichita State University.

All other work conducted for the thesis was completed by the student independently.

Funding Sources

No source of funding was provided.

NOMENCLATURE

Al	Aluminum
AWG	Aerospace Working Group
EPP	Expanded Polypropylene
FAA	Federal Aviation Administration
FE	Finite Element
FW	Fixed-Wing
MNC	Metallic Corrugated Nosecone
MT	Metallic Corrugated Tubes
NIAR	National Institute for Aviation Research
PCB	Printed Circuit Board
PUR	Polyurethane
t	Time
TAMU	Texas A&M University
TO	Topology Optimization
UAS	Unmanned Aerial System

TABLE OF CONTENTS

Page

LIST OF FIGURES

FIGURE Page

LIST OF TABLES

TABLE Page

1. INTRODUCTION

1.1 Introduction

Small unmanned aerial systems (UASs) have seen a significant increase in their use for hobby-flying, surveillance, aerial deliveries, geo-mapping, infrastructure inspection, and other operations. As per the Association for Unmanned Vehicle Systems International, the UASs industry is expected to have a positive economic impact of $82 billion on the US economy by 2025 [1]. The Federal Aviation Administration (FAA) has predicted an increase in the small UAS population from 1.25 million units in 2018 to 1.66 million units by 2023 in the US [2]. FAA classifies small UASs as those weighing < 25 kg (55 lb) [3]. The safe integration of the growing UAS population into the national airspace is challenging due to an increase in UASs sightings in the restricted airspace [4–6] and several events involving UAS collisions with manned aircraft [7–10]. These scenarios can be dangerous and have encouraged research to assess the severity of small UASs collision against manned aircraft. Small UAS collisions are found to be more severe than bird strikes and can cause critical damage to the aircraft structures [11–18]. UAS collision damage severity is attributed to the use of hard materials, rigid and high-density components, and their relative placement [12, 14–20]. [11–18] demonstrate serious flight safety concerns in UASs airborne collisions with manned aircraft. There is a need to develop UASs that are less damaging in these scenarios along with implementing 'detect and avoid' technologies to minimize the possibility of such events for safer airspace.

Airborne collision simulations performed by Olivares *et al.* [16] predicted that a fixed-wing UAS in its tractor configuration (motor located at the front of the fuselage) can severely damage commercial and business jet aircraft primary structures upon 128.6 m/s (250 knots) impacts. The UAS can perforate the aircraft skin and damage the underlying load carrying structures. These studies also provided the following insights: 1) the motor in the front acted as a sharp penetrator and perforated the target allowing large portions of the UAS to pass through the target, 2) most

of the damage was caused due to the heavy, rigid, and high-density UAS components (motor, battery, and payload) which remained mostly intact after perforating the target and retained significant momentum, and 3) the in-line arrangement of these heavy and rigid components caused multiple target impacts along the axis of impact. Based on these observations, this thesis primarily focuses on developing design concepts for a small fixed-wing UAS that mitigate impact damage to aircraft primary structures at such high velocity. The baseline tractor engine configuration of Precision Hawk Lancaster Hawkeye Mark III UAS [19] was modified into a pusher engine configuration (motor located at the aft of the fuselage) as part of this work. The details of tractor and pusher configurations are discussed in Sections 1.2 and 2.2 of this work. Finite Element (FE) impact simulations of the pusher UAS against a 1.59 mm thick stiffened aluminum flat-plate target that represents typical aircraft skin were performed using LS-DYNA to explore frangible design concepts. For mitigating the impact damage, a fixed-wing UAS pusher configuration was developed that included an energy absorbing polymeric nosecone in the front of the UAS. The preliminary investigation was performed on nosecones of various polymers - expanded polypropylene (EPP) [21], polyurethane (PUR) [22], and polystyrene based 'IMPAXX700' [22] foams for better energy absorption. Conventional conical and semispherical nosecone geometries were considered for the preliminary evaluation of the pusher configuration and subsequently, a topologically optimized nosecone was designed for improved impact energy absorption. Also, a payload drop mechanism was designed and implemented into the UAS to avoid multiple impacts along a single axis against the target. Finally, lightweight, energy absorbing, corrugated Al structures were implemented into the proposed UAS design which eliminated the target plate tearing. These designs will be discussed in detail in Chapter 2 of this thesis. Part of the work on polymeric nosecones and payload drop mechanism can also be found in [23]. The frangible fixed-wing UAS FE model was then provided to the Wichita State University, National Institute for Aviation Research (NIAR) for re-assessing the worst case air-to-air collision scenarios between the UAS, and commercial and business jet aircraft [16, 19] to evaluate the effectiveness of the frangible design in damage reduction.

This thesis is primarily focused on the structural design aspects to mitigate UAS impact severity and acknowledges that the changes introduced can compromise UAS performance on certain metrics (engine efficiency, aerodynamics, endurance, *etc.*).

1.2 Background

A FE model of the 1.8 kg (1812 g) fixed-wing UAS Precision Hawk Lancaster Hawkeye Mark III (original tractor configuration) shown in Figure 1.1 was developed by Kota [19] for evaluating airborne collision severity between the fixed-wing UAS and commercial and business jet aircraft as a part of the FAA's ASSURE program [24]. The fixed-wing UAS is constituted of a fuselage (487 g) - primarily constructed of printed circuit boards (PCBs) as the major structural components, polymeric wings (370 g), composite tail booms connecting the tail portion (143 g) to the fuselage, motor (80 g), battery (340 g), payload (395 g), and certain electronic chips, connectors, servo motors, and sensors. In the tractor configuration, the motor was attached to a firewall in the forward fuselage. Battery and payload were located aft of the motor; all in an almost in-line arrangement. The Motor, and battery and payload were supported by PCB casings as shown in Figure 1.2.

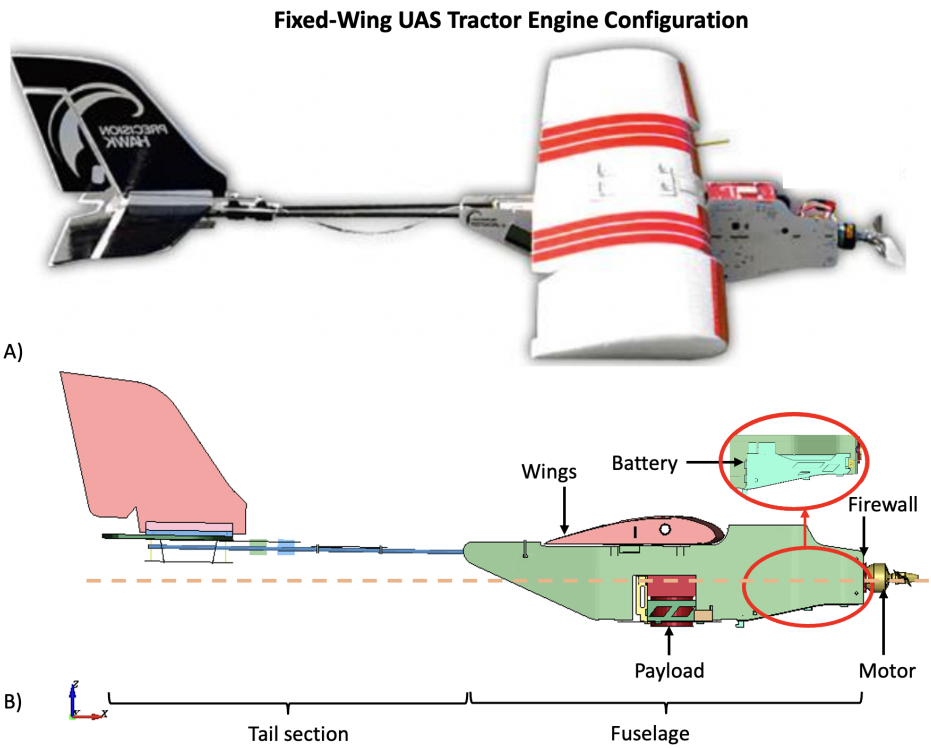

Figure 1.1: A) Precision Hawk Lancaster Hawkeye Mark III UAS (adapted from [19]) and B) corresponding FE model in the original tractor configuration.

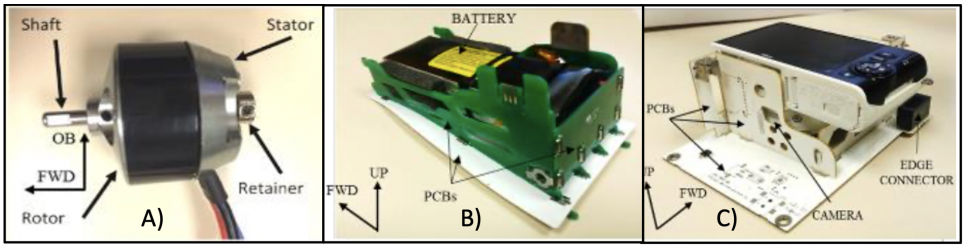

Figure 1.2: Precision Hawk UAS components A) motor, B) battery, and C) payload (reprinted from [19]).

Kota *et al.* [19] developed the UAS tractor FE model. They performed component level impact tests for the motor and battery against Al 2024-T3 flat-plate target for validation of the FE models of critical UAS components. High fidelity motor and battery FE models were included in the full

scale UAS FE model. The full model was then used to simulate impacts against deformable and rigid Al flat-plate targets. In the predicted impacts, the motor shaft perforated the target with the motor passing through the target mostly intact. The size of the perforation increased as the rest of the UAS perforated through and most of the heavy components such as the battery and payload remained intact after perforating the target. These components retained significant momentum capable of causing substantial damage to underlying aircraft structures (ribs, spars, *etc.*).

Air-to-air impact simulations were performed between tractor UAS and aircraft primary structures [16, 19] (wing-leading edge, horizontal and vertical stabilizers, and windshield) after verifying FE model for numerical stability against rigid flat-plate and rigid knife-edge targets. A severity index was developed by the NIAR [16] for evaluating the severity of these collisions based on the damage to a given aircraft structure. The severity index was defined from level I-IV with level IV being the most severe. Level IV severity index was identified for certain collision scenarios [16,19], which typically resulted in UAS perforating the aircraft skin and damaging underlying structures. Further details of the work can be found in [16, 19, 20]. This thesis investigates the possibility of reducing air-to-air impact severity between UASs and manned aircraft by developing a frangible pusher UAS configuration. The approach and design modifications for developing the frangible design are described in Chapter II.

2. DESIGN OF A FRANGIBLE FIXED-WING UAS *

2.1 Introduction

Small UASs are increasingly used for commercial, surveillance, and hobby purposes. The Federal Aviation Administration (FAA) has predicted an increase in small UASs from 1.25 million units in 2018 to 1.66 million units in 2023 [2]. The FAA classifies small UASs as those weighing < 25 kg (55 lb) [3]. The rise in small UASs population poses a big challenge to safely incorporate them into the national air space. There has been an increase in the reported UASs sightings in restricted airspace [4–6] along with numerous instances of UASs near-miss and collisions with manned aircraft [7–10] in the last decade. This has motivated evaluation and quantification of the potential damage caused by such events. The FAA has prioritized the evaluation of airborne collisions between UASs and manned aircraft to safely incorporate UASs into national airspace [25, 26]. Small UAS's airborne collisions to manned aircraft have been considered analogous to bird strikes [14–17,27,28], as existing aircraft airworthiness certifications have defined bird strike damage thresholds with respect to either the mass or the impact energy of the bird [29–31]. Small UAS collisions are more severe than bird strikes and can cause critical damage to the load bearing structures [11–18]. UAS collision damage severity is attributed to the use of hard materials, rigid and high-density components, and their relative placement [12, 14–20]. Olivares *et al.* [15, 16] performed finite element (FE) simulations for airborne collision severity evaluation with a 1.2 kg (2.7 lb) quadcopter and a 1.8 kg (4 lb) fixed-wing UAS against commercial and business jet aircraft primary structures (wing leading edge, vertical and horizontal stabilizer, and windshield). The simulations demonstrated that UAS collisions can cause substantial damage to the aircraft structures, penetration of their outer skins, and ingress of UAS components that collide against internal air-frame components. Scaled up UAS impacts involving a 1.8 kg quadcopter and a 3.6 kg (8 lb) fixed-wing UAS were also simulated to compare against equivalent mass bird strikes.

*Part of this chapter is reprinted with permission from "Development of a frangible design of small fixed-wing unmanned aerial system" by Anurag, K. R. Kota, T. E. Lacy, 2021. *In Proceedings of the American Society for Composites - 36th Technical Conference*, Copyright 2021 DEStech Publications, Inc.

The UAS collisions were more severe than equivalent bird strikes due to their hard, dense, rigid components, and their discrete mass distribution. Meng *et al.* [13] assessed the damage caused by a 3.4 kg (7.5 lb) quadcopter collision against a commercial airliner horizontal stabilizer through experiments and validated FE simulations. Such collisions at a cruising speed of 151 m/s would prevent a safe flight due to damage to the horizontal stabilizer front spar. The British Military Aviation Authority, the Department for Transport (British), and the British Airline Pilots' Association commissioned a study for evaluating collision scenarios between drones (*i.e.,* quadcopters and fixed-wing UASs) and helicopters and airliners primarily focused on the windscreens [11] involving experiments and FE modeling. They concluded that the drones can critically damage helicopter windscreens in realistic scenarios; even airliner windscreens can be severely damaged with a 4 kg (8.8 lb) class quadcopters and a 3.5 kg (7.7 lb) class fixed-wing UASs at high but realistic speeds. Such impacts inhibit safe flight. Lyons and D'Souza [14] performed business jet engine ingestion simulations comparing the severity of a 1.2 kg quadcopter with a 1.2 kg bird; the quadcopter ingestion was significantly more damaging to the engine blades. The effects of the phase of the flight (take-off, cruise, and landing), impact location and orientation, and thickness of fan blades on damage development were investigated. The damage severity was attributed to the hard quadcopter components. These earlier works document the serious threat to flight safety and argue that the sole reliance on the UAS 'detect and avoid' technologies is flawed. A review of 600 small UASs by Deaton [32] revealed that the current collision avoidance systems for aircraft cannot be implemented on small UASs and there is a need for novel collision avoidance systems. This necessitates the development of frangible UAS designs to minimize the air-to-air collision damage to ensure safer airspace.

This work aims to develop a frangible design for a nominal 1.8 kg Precision Hawk Lancaster Hawk Eye Mark III fixed-wing UAS to mitigate airborne collision damage to aircraft by avoiding the target plate (representative of aircraft typical skins) tearing at an impact velocity of 128.6 m/s (250 knots). This is achieved using LS-DYNA FE impact simulations between modified fixed-wing UASs and an Al flat-plate target. The original Precision Hawk 'tractor' engine configuration

(motor as the foremost part of the UAS, Figure 2.1 (A)) was redesigned into a frangible 'pusher' engine configuration (motor mounted to the aft of the fuselage, Figure 2.1 (B)) [19]. In the tractor configuration, the motor was the foremost component of the UAS followed by the battery and payload among the other heavy and stiff UAS components, in an almost in-line arrangement. The earlier study on fixed-wing UAS impact simulations using the tractor configuration [19] demonstrated: 1) the motor shaft effectively acted as a sharp penetrator during tractor configuration impacts to semi-monocoque metallic targets, typically perforating the target allowing the other hard UAS components to pass through the perforated structure mostly intact with minimal momentum loss; 2) the motor, battery, and payload were the major damage-causing components due to their high density, relatively stiff structure, and nearly in-line arrangement that caused multiple impacts on the target along the same axis. The frangible design was prima facie based on these observations and a pusher configuration was designed with the motor aft of the fuselage, rear of the battery and payload maintaining the in-line arrangement. Energy absorbing polymeric nosecone was introduced in the UAS front in place of the motor. This frangible pusher configuration was used as a baseline to simulate UAS impacts against flat-plate targets. Further details of the UAS configurations and FE model are discussed in Section 2.3. The flat-plate target was a 1.59 mm thick Al 2024-T3 sheet, representative of typical aircraft skin, sandwiched between a rigid target frame [16, 19, 20]. The impacts were simulated at 128.6 m/s (250 knots). This relative velocity corresponds to typical impacts between fixed-wing UASs and manned aircraft operating at altitudes of less than 4000 m [19, 20]. The payload velocity for the duration of impact (including residual velocity after target perforation) and target plate strain were used as the main criteria for evaluating the impact damage.

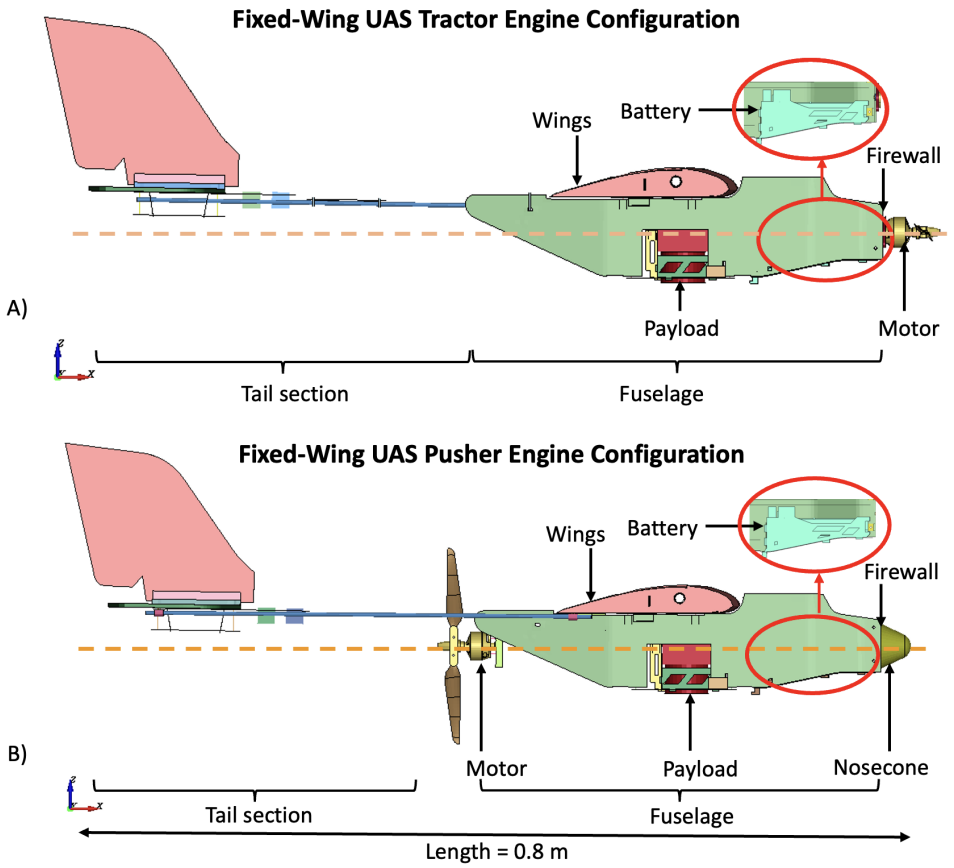

Figure 2.1: FE model of fixed-wing UAS A) tractor B) pusher configuration with conical nosecone.

A series of design iterations were performed for mitigating the impact damage to the flat-plate target. Initial iterations were performed with energy absorbing polymeric foam nosecones attached to the front of the UAS. Polymeric foam material (expanded polypropylene (EPP) [21], polyurethane (PUR) [22], polystyrene based 'IMPAXX700' [22]) and geometry (conical and semi-spherical) evaluations were performed for the nosecone to identify the best design in mitigating the target damage. Next, a payload drop mechanism, inspired by the engine drop concept in automotive frontal crashes, was designed for the UAS to divert the payload (the heaviest component) out of the line of the single-axis impact of the battery and motor. Also, the nosecone geometry was topologically optimized to improve the impact energy absorption. These designs significantly reduced the impact damage to the target compared to the baseline configuration impacts by lower-

ing the payload velocity after target perforation, but the fragmented UAS components still passed through. To completely avoid target plate tearing, metallic crushable structures inspired by automotive crush tubes were then designed to further increase the impact energy absorption. Metallic crushable corrugated tubes (MT) mounted between the battery and payload, and a metallic crushable corrugated nosecone (MNC) mounted to UAS front, both made of Al 6061-T6, were evaluated for impact damage reduction. This design succeeded in avoiding the target plate tearing and was chosen as the frangible design. This frangible FE model was then verified for numerical stability and robustness. The details are discussed in the following sections. The frangible design was then used to re-assess the worst case tractor UAS airborne impacts to commercial and business jet aircraft identified from [16, 19]. This work is being performed in association with the Wichita State University, National Institute for Aviation Research (NIAR) to evaluate the effectiveness of frangible design in air-to-air collision scenarios.

The authors acknowledge that the design modifications made to the UAS for mitigating the impact damage will result in a trade-off between the UAS performance (engine/motor efficiency, aerodynamics, endurance, *etc.)* and impact damage mitigation. The pusher UAS configuration designed in this work is similar to small UASs like a 2.9 kg VAMP UAS [33], a 0.3 kg CAMFLYERG [34], *etc.* with a similar construction but there are other small fixed-wing UAS pusher configurations [35–37] that can be explored for impact damage reduction. These configurations will differently affect UAS performance and influence their systems design, speculating one can be better than the other. However, this thesis is focused on the structural design aspects for reducing impact damage to targets and the design concepts discussed will still be applicable.

2.2 The UAS and FE Model Description

The original 1.8 kg (1812 g) Precision Hawk UAS was constituted of a fuselage (487 g) - primarily constructed of printed circuit boards (PCBs) as the major structural components, polymeric wings (370 g), composite tail booms connecting the tail portion (143 g) to the fuselage, motor (80 g), battery (340 g), payload (395 g), and certain electronic chips, connectors, servo motors, and sensors. It had tractor configuration with the motor as the foremost component. The pusher

configuration UAS design weighed 1763 g compared to the 1812 g tractor configuration. The center of gravity (CG) for the pusher UAS design was identical to the tractor. For example, the CG for the pusher configuration (with conical nosecone) was given by x= -313.40 mm, y= 1.00 mm, z= 13.68 mm whereas for the tractor configuration the CG was located at x= -307.27 mm, y= 0.74 mm, z= 14.23 mm relative to the origin of the global coordinate system. The UAS FE models for the tractor and pusher configurations were extracted from [19]. Most of the UAS components were modeled using shell and solid FEs, with bolts being modeled using 1D beam FEs. A nominal mesh size of 5 mm was used for the shell and solid FEs. The minimum element size was kept to 1 mm to capture smaller features and ensure model fidelity while maintaining reasonable simulation run times. The mesh quality criteria defined by the NIAR [19] was used for modeling the components as described in Table 2.1. The baseline pusher UAS model had 29243 shell FEs, 65550 solid FEs, and 50 beam FEs.

Table 2.1: Mesh quality parameters (reprinted from [19]).

Quality parameter	Shell elements	Solid elements
Minimum side length	1 mm	1 mm
Maximum aspect ratio	5	5
Minimum quad angle	45^o	-
Maximum quad angle	140^o	-
Minimum tria angle	30^o	-
Maximum tria angle	120^o	-
Maximum warp angle	15^o	15^o
Minimum jacobian	0.7	0.5

CONTACT_ERODING_SINGLE_SURFACE was used for the UAS system and for the target system *CONTACT_AUTOMATIC_SINGLE_SURFACE* was used. Among the two systems (the UAS and the target), *CONTACT_ERODING_SURFACE_TO_SURFACE* was used. The static and dynamic friction coefficients *FS* and *FD* for these contacts were assumed to be 0.2. Detailed contact card information for individual parts can be found in [19]. The impact simulations were

performed using LS-DYNA version R12.1.0 and had a run time of ∼4.5 hrs using 8 CPUs. The impacts were simulated for a duration of 7 ms.

The flat-plate target FE model was provided by the NIAR in which the Al plate was sandwiched between a rigid target frame. The rigid target frame was completely constrained at the four corners. The target plate modeled using shell FEs was attached to the target frame modeled using solid FEs through bolts modeled using beam FEs. The *MAT_057 MAT_JOHNSON_COOK* material model was used to model the Al 2024-T3 flat-plate. The UAS FE model impact setup is shown in Figure 2.2.

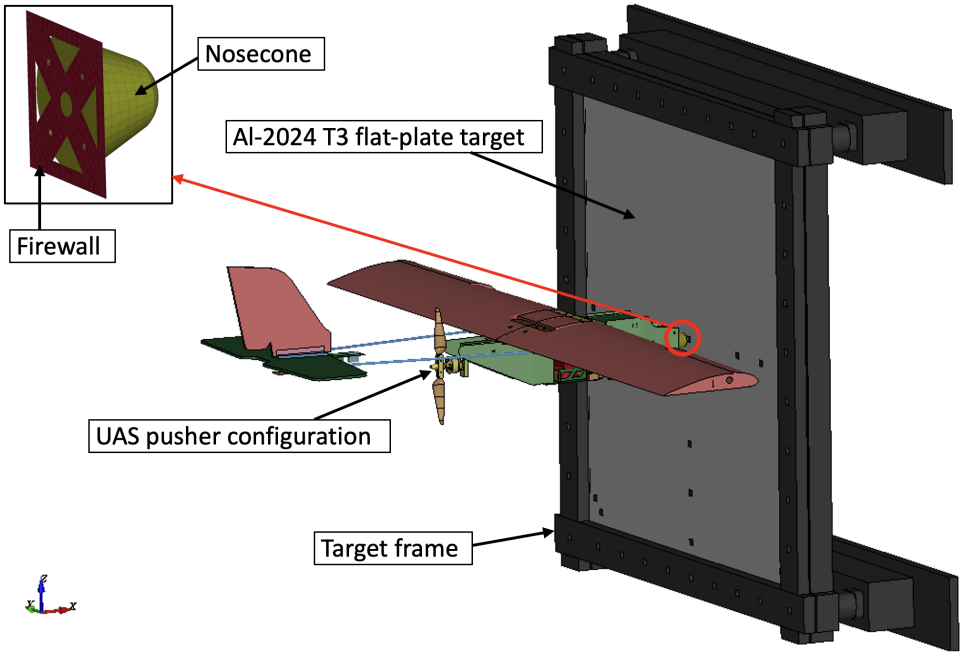

Figure 2.2: FE model setup for impact simulation with UAS pusher configuration (baseline) against the flat-plate target. (Nosecone attached to firewall in the inset).

2.3 Frangible UAS Design Concepts

2.3.1 Polymeric Foam Nosecone for Frangible UAS Design

Energy absorbing polymeric foam nosecones were designed for the UAS, attached to the firewall in front in place of the motor to mitigate impact damage. Three low density polymeric foams

were reviewed for the nosecone material based on their compressive stress-strain behavior: 1) expanded polypropylene (EPP) foam [21] - used in helmets and packaging goods, 2) polyurethane (PUR) foam [22] - used in automotive doors and panels, and 3) polystyrene based 'IMPAXX700' foam [22] - used for commercial impact attenuators complying with Formula Society of Automotive Engineers regulations. The density and Young's modulus of these foams are listed in Table 2.2. Based on their compressive stress-strain curves (Figure 2.3), IMPAXX700 foam had higher energy absorption per unit mass, which was used as the nosecone material.

Table 2.2: Properties of polymeric foams.

Polymeric Foam	**Density (Kg/m^3)**	**Young's Modulus (MPA)**
EPP [21]	60	0.98
PUR [22]	60	0.16
IMPAXX700 [22]	45	42.5

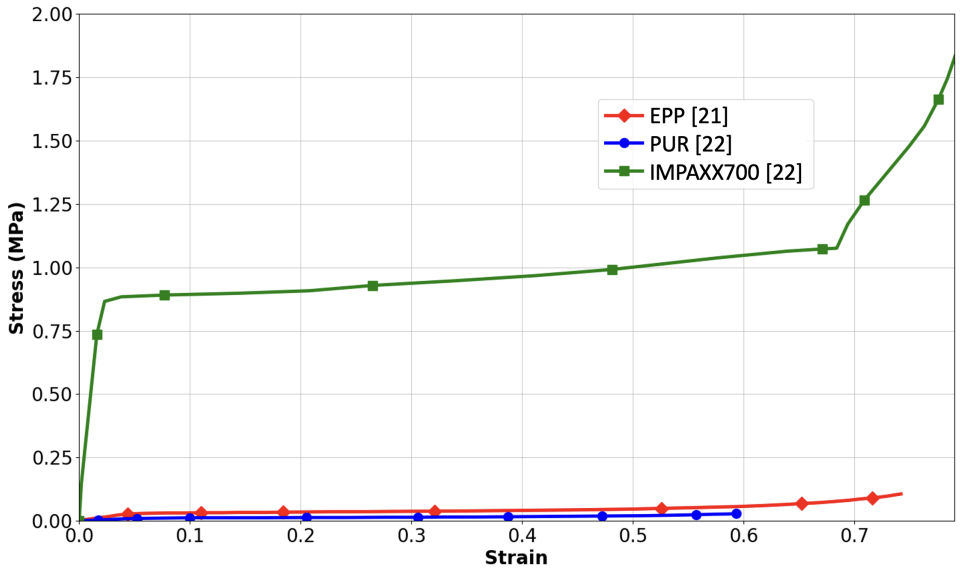

Figure 2.3: Compressive stress strain behavior of EPP [21], PUR [22], and IMPAXX700 [22] foams.

IMPAXX700 foam was modeled using the *MAT_057 MAT_LOW_DENSITY_FOAM* [38, 39] material model used to model low density and high energy absorbing foams. The foam response was verified to match experimental data [22] by performing a simplified compression test simulation with a 50 mm cubical foam block model at a strain rate of 0.1 s^{-1}. As IMPAXX700 foam is insensitive to strain rate [40], the same response was used for high speed UAS impact simulations at 128.6 m/s. The predicted response showed a good correlation with the experimental data as seen in Figure 2.4.

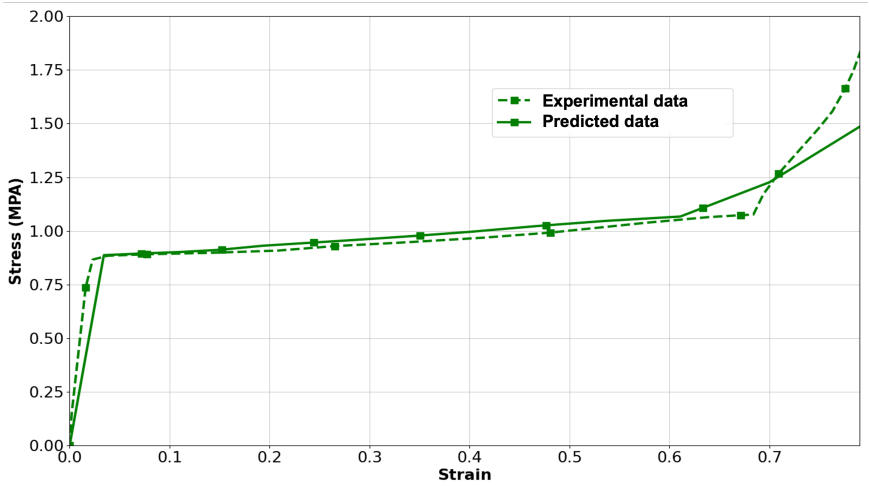

Figure 2.4: Benchmarked stress-strain curve for IMPAXX700 foam [22].

Conventional conical and semispherical geometries were studied for nosecone design (Figure 2.5). Nosecones had a base diameter of 56 mm and a height of 45 mm, approximating the motor dimensions. The nosecones were modeled using solid FEs. The nosecone was attached to the UAS firewall using four bolts modeled as beam elements.

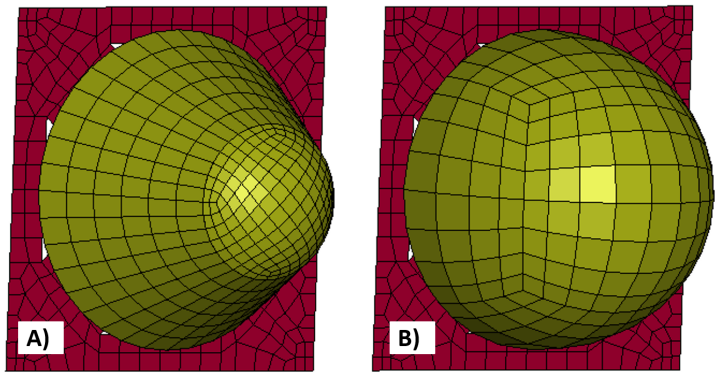

Figure 2.5: FE models of A) conical and B) semispherical nosecones.

Full scale UAS impact simulations were performed using conical and semispherical geometries where the conical nosecone proved to be better in reducing the damage severity. The UAS perforated the target, however, the residual payload velocity (at t= 7 ms) in the case of the UAS with conical nosecone was about 54% lower compared to the tractor configuration impact (Figure 2.6). This residual payload velocity was considerably higher and can cause substantial damage to subsequent structures after target perforation. Thus, a payload drop mechanism was devised to divert the payload impact trajectory and minimize target damage.

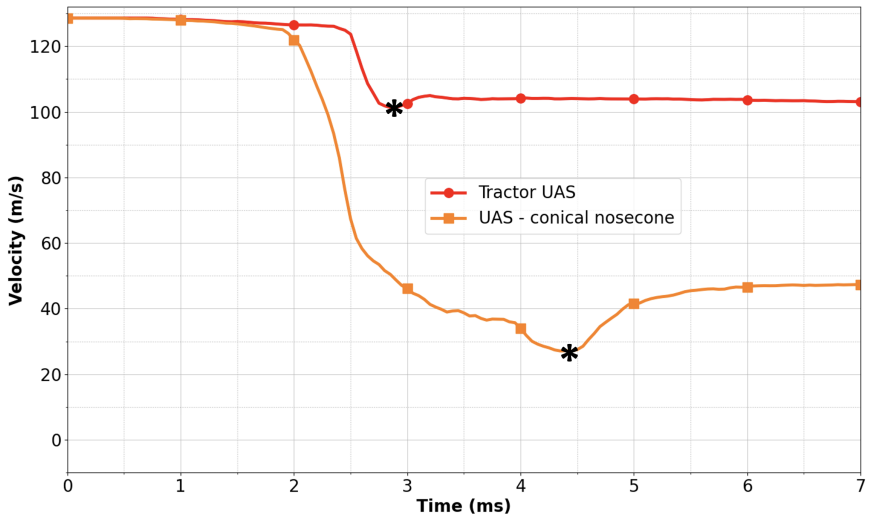

Figure 2.6: Payload velocity comparison for impact duration. ('*' represents the instant when the payload perforates through the target).

2.3.2 Payload Drop Mechanism Design for Frangible UAS

A payload drop mechanism was designed for the frangible UAS along with the conical nosecone. It was inspired by mass decoupling and energy absorption structural design concepts for frontal crashes in automobiles where the engine mounts are either sheared off or the structures collapse in a way that makes the engine move down. This limits the energy transfer to and peak impulse experienced by occupants. The payload drop mechanism diverted the payload trajectory upon impact to avoid its single-axis impact with the battery and motor. It was based on two major concepts:

1) Shearing of payload mount bolts: Existing Nylon 6 [19] payload mount bolts were modified to reduced neck bolts and gripped an Al 7075-T6 linear link extending from the firewall to the payload mounts (Figure 2.7 (A)). The linear link transmitted the high impact force directly to bolts at the reduced area, ensuring desired bolt failure.

2) Pushing payload down upon collision: A relatively stiff angled structure ('⌋'-shaped) free to rotate on a bearing (Figure 2.7 (B)) was designed to push the payload down, both made from Al 7075-T6 [41]. Another Al 7075-T6 linear link extending from the top of the firewall was connected to the upper leg of the angled structure and the lower leg of the angled structure was positioned on top of the payload. The linear link transferred the impact motion directly to the angled structure, which being free to rotate, pushed the payload down. The bearing of the angled structure was modeled using a disc and a revolute joint in the simulation.

All the linear links were designed slender, to buckle during the impact, and avoid additional damage. The integration of the payload drop mechanism into the UAS is shown in Figure 2.8. The *MAT_024 MAT_PIECEWISE_LINEAR_PLASTICTICY* material model was used for modeling Al 7075-T6 and Nylon 6. The angled structure was modeled rigid using the *MAT_020 MAT_RIGID*. Tied contacts (*CONTACT_TIED_NODES_TO_SURFACE*) and bolts were used to attach the components to the UAS.

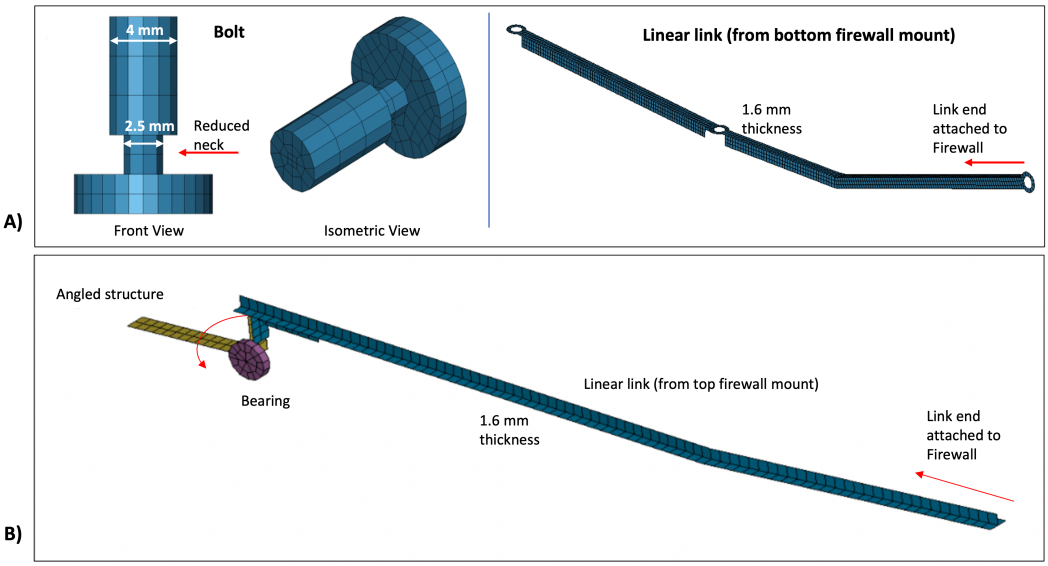

Figure 2.7: A) Reduced neck bolts and linear link for shearing payload mount bolts and B) mechanism for deviating the payload impact trajectory.

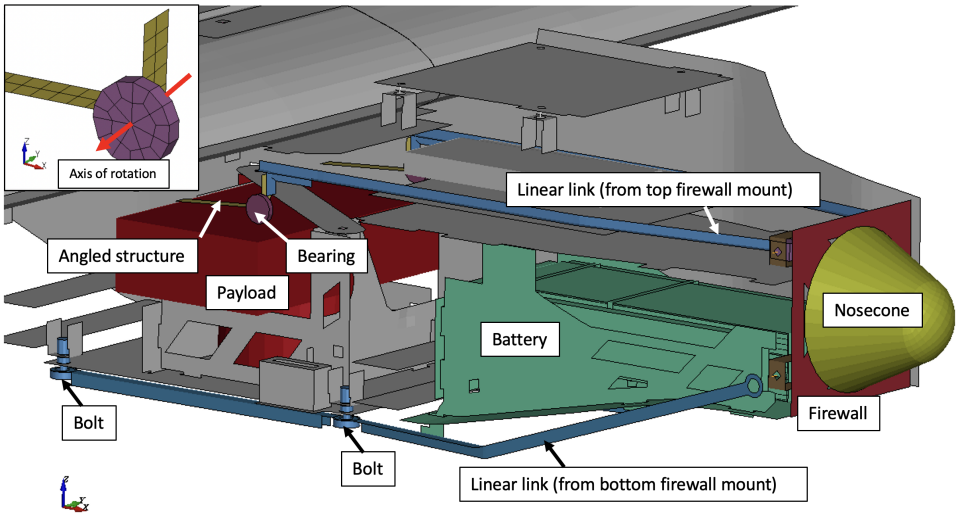

Figure 2.8: Integration of payload drop mechanism into UAS. Revolute joint for angled geometry in the inset.

Simulated impacts with the payload drop mechanism predicted a more benign impact with about 59% decrease in payload residual velocity at 7 ms after target perforation compared to tractor

configuration impact (Figure 2.9). However, the relative reduction in residual payload velocity with and without the payload drop mechanism was not large ($\sim$ 10%). This is due to very high velocity impact which gives minimal time for the payload drop mechanism to act effectively. The residual payload impact velocity is still high and the target plate was perforated. Thus, nosecone topology optimization was performed combined with different nosecone lengths to improve its impact energy absorption with optimum mass in an attempt to avoid target plate perforation.

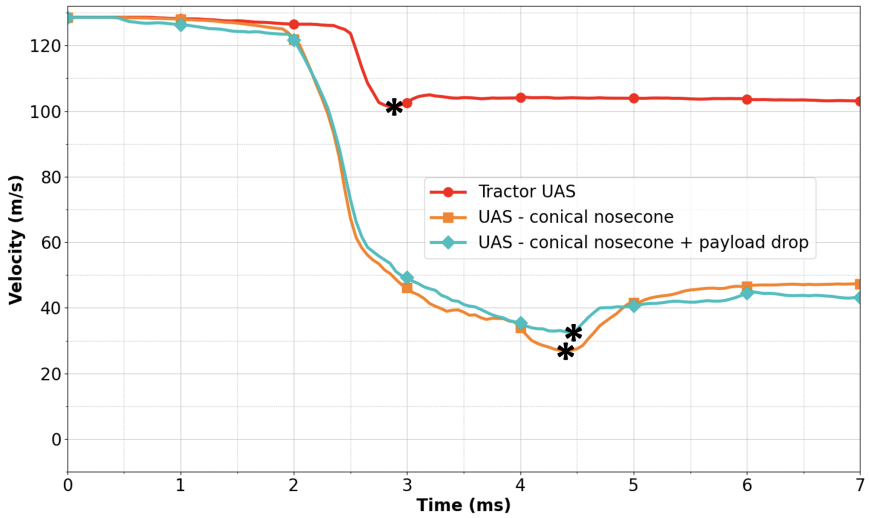

Figure 2.9: Payload velocity comparison for impact duration. ('*' represents the instant when the payload perforates through the target).

2.3.3 Topology Optimized Nosecone for Frangible UAS Design

2.3.3.1 Nosecone Topology Optimization

Topology optimization (TO) is used to find the optimal layout of the structure *i.e.,* where the material should be located to support the desired load. In TO, a domain for optimization, boundary conditions, and mass constraint are required as inputs. The optimizer tool tries to find the best material layout in the domain by maximizing the structure's stiffness (minimizing the compliance) which equates to minimizing the external work, meeting the mass constraint. When FE method is used for TO, each element is assigned its own density, stiffness, and other material properties

which represent the design variables. These design variables are dependent on relative density, x, which is the primary design variable used to parameterize the material properties. In general, the TO problem can be formulated as:

$$min_{\mathbf{x}} f(\mathbf{x}),$$

subject to,

$$\sum_{i=1}^{N} \rho(x_i) V_i \leq M^*$$

$$x_{min} \leq x_i \leq 1$$

$f(\mathbf{x})$ is the objective of the problem *i.e.,* minimization of external work, V_i is the volume of the i^{th} element, $\rho(x_i)$ is the density of the i^{th} element, M^* is the target mass, and N represents the total number of elements. x_i is the relative element density which ideally varies from 0-1 but for numerical stability, it is assigned a lower bound close to 0. Since the element density is dependent on the relative density, elements can have intermediate densities which is practically infeasible. To avoid such behavior, the elements are derived either to be fully used or not to be used at all using material interpolation algorithms. A general material interpolation algorithm [42] can be formulated as:

$$\rho(x) = x\rho_0$$

$$E(x) = xE_0$$

$$\sigma(x) = x^p \sigma_0$$

$$E_h(x) = x^q E_{h0}$$

where ρ denotes the density of the material, *E* represents the Young's modulus, σ is the yield stress, E_h is the strain hardening modulus, p and q are exponents. The subscript '0' refers to the base material properties. The values of the exponents can be varied to help in the stability of the

solution.

Comprehensive work on TO methods can be found in the works of Rozvany [43] and Bendsøe and Sigmund [44]. Conventionally, TO has been performed for linear static problems [45, 46] using gradient-based methods that calculate analytical sensitivities. However, for non-linear dynamic problems like crash-worthiness, the gradient-based approach is not suitable due to changing boundary conditions, and material and geometric non-linearities. Calculating sensitivity information for such problems will be highly expensive and practically infeasible, thus, alternative approaches like heuristics based methods [47, 48], optimality criteria [42] *etc.* have been developed. In this work, LS-TaSC optimization software has been used for nosecone TO which has optimality criteria and projected subgradient methods capable of handling non-linear dynamic problems [42]. The projected subgardient method is proven to work faster than the optimality criteria yielding similar results [42] and was chosen in this work. For material interpolation, the True Mechanics approach available in LS-TaSC was used which is recommended for non-linear dynamic problems [49].

Nosecone TO was used to achieve the best geometry for absorbing the maximum impact energy with a given weight to contribute to our bigger objective of determining the ideal nosecone shape and size for minimizing the impact damage. For determining the size dimensions, topology optimization was combined with manual iterations for different lengths of the nosecone. The topology optimized nosecone was then modified to account for aerodynamic considerations. The details of the nosecone TO are described in the following sections.

2.3.3.2 Nosecone Topology Optimization FE Model Setup

Three cylindrical domains with lengths 50, 78, and, 100 mm, each of a diameter 72 mm were considered for TO. The diameter was chosen based on the maximum mounting space available on the firewall. A mass fraction of 0.4 was chosen as the baseline for the optimization. With a 78 mm long cylinder as the reference, sensitivity studies using 0.4 and 0.5 mass fractions, and 5 mm and 2.5 mm mesh sizes were performed which yielded similar optimization results. To reduce optimization run-time, the UAS model was modified to remove the tail portion and wings along with modifying the target frame model to reduce element count without altering the boundary condi-

tions. This considerably shortened the iteration run-time to 2 hrs. The initial nosecone domain and UAS FE optimization setup are shown in Figure 2.10. LS-TaSC TO parameters are shown in Table 2.3.

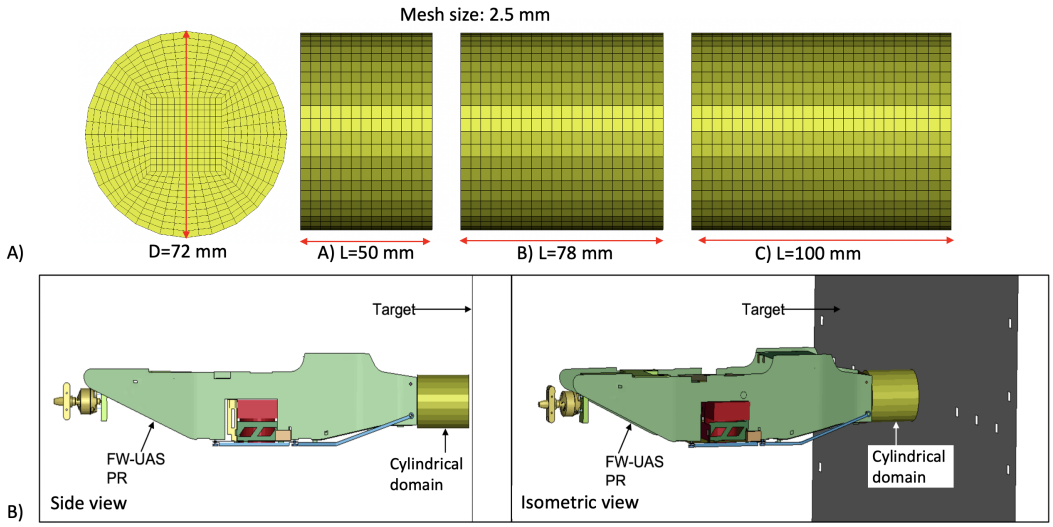

Figure 2.10: A) Cylindrical domains and B) simplified UAS impact FE setup for nosecone TO.

Table 2.3: Topology optimization parameters.

LS-TaSC version	LS-TaSC\4.2
Iteration time	2 hrs
Max. iterations	15
No. of Processors	8
Method	Projected subgradient
Mass fraction	0.4
Desired mass flow	2*default
Descent acc. factor	2*default

The optimization for the three cases (50, 78, and 100 mm long cylinders) converged in 9-10 iterations. The optimized shapes are shown in Figure 2.11. The following observations were made from the optimized shapes:

1. Optimized shapes had a similar geometric pattern with more mass towards the bottom of the cylinder, in-line with the heavy UAS components: battery and payload.

2. The optimized cylinders retained the original length in all cases, this is to maintain the same boundary conditions.

3. Optimized cylinders were impractical for aerodynamic considerations.

4. The volume for the optimized cylinders was 76339, 118084, and 153843 mm^3 for the 50, 78, and 100 mm cylinders, respectively.

The 78 mm optimized cylinder was chosen as the optimal design based on mass addition to UAS. For aerodynamic purposes, a hollow nosecone (Figure 2.12) with a concentrated mass on the lower portion consistent with the optimal cylinder and with an outer contour motivated by sailplane geometry [50] was designed.

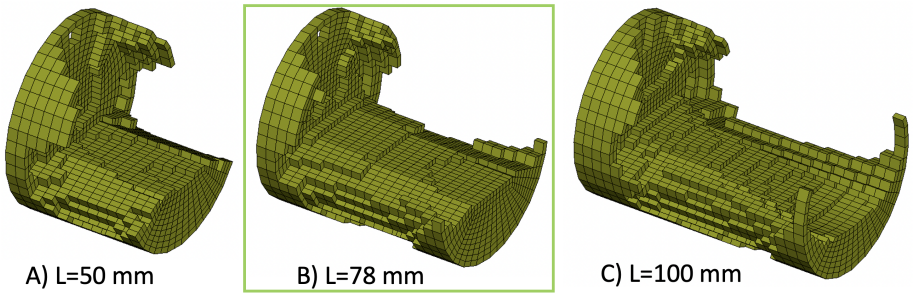

Figure 2.11: Optimized cylindrical shapes from LS-TaSC for A) 50, B) 78, and C) 100 mm lengths.

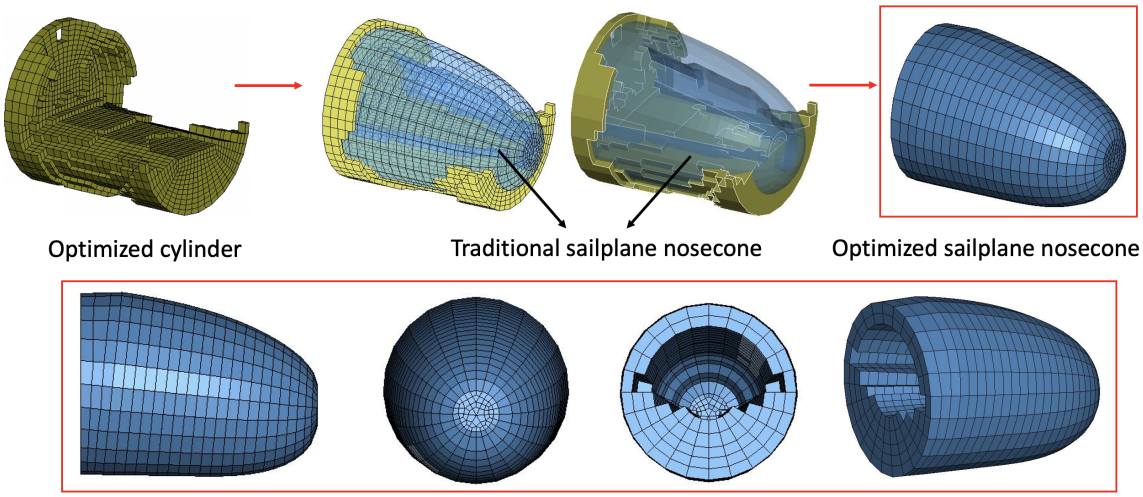

Figure 2.12: Optimized cylinder to practical sailplane design.

2.3.3.3 UAS Impact Simulation Results with Optimized Nosecone

The optimized nosecone replaced the conical nosecone in the UAS frangible design with the payload drop mechanism. The simulated impacts with the optimized nosecone still predicted target plate tearing. However, a 78% and a 46 % decrease in payload residual velocity (t= 7 ms) was observed compared to the tractor configuration and the UAS with conical nosecone and payload drop mechanism respectively (Figure 2.13). This residual velocity was very low but to avoid target plate tearing, higher energy absorbing structures were desired, which caused a shift towards metallic crushable structures. The corrugated metallic crushable structures avoided any target plate tearing. Their detailed design is explained in Section 2.5 of this work.

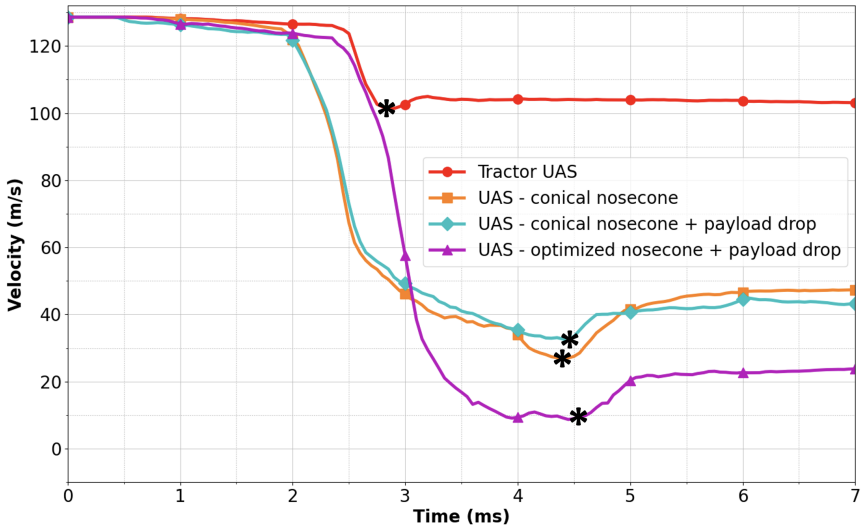

Figure 2.13: Payload velocity comparison for impact duration. ('*' represents the instant when the payload perforates through the target).

2.4 Frangible UAS Design with Energy Absorbing Metallic Structures

Crushable metallic structures [51–53] are used in automotive applications to absorb energy during impact like crush cans behind bumper beams for low velocity impacts and longer crush rails for absorbing high velocity impacts. These help to absorb impact energy while limiting the peak forces by maximizing the area under the force-displacement curve for improved energy absorption. Since metals are a lot stiffer than polymeric foams they absorb significantly higher energies during elastic-plastic deformations. Their structural configurations can be designed such as to keep their mass low. Sahu and Gupta [51] studied the crush can behavior of 1.2-1.75 mm thick Al cylinders open from both sides with corner short-dent, corner long-dent, mid-dent configurations along with thickness variation in the crush zone for automotive bumpers and concluded that long dents provided smoother energy absorption with force-displacement curves closer to rectangular shapes. Yuen and Nurick [52] provided an extensive review of axial crushing behavior of modified tubular sections with imperfections such as corner indentations, mid-dents, long-dents, corrugated tubes, *etc.*, along with filled tubes and material modifications. Zhou *et al.* [53] studied the crushing behavior of slotted rectangular tubes made of steel for energy absorption under axial loading and

found that slotted tubes reduced the peak forces. They also studied the cracks in the failed tubes and how they affect the energy absorption.

Based on such concepts, energy absorbing Al crushable structures were designed: Al corrugated tubes and an Al corrugated nosecone to avoid the target plate tear.

2.4.1 Design of Rectangular Metallic Corrugated Tubes (MT)

Two hollow metallic corrugated tubes (MT) made of Al 6061-T6 were mounted between the battery and payload (Figure 2.14). The cross-section of the individual tubes was rectangular and they had a flat panel attached in front and back connecting the two to uniformly distribute the impact load and provide a smooth mounting surface. MT were designed per the space availability and had a length of 55 mm with three corrugations along the length for the desired buckling of the structure. The design was iterated for corner dents, slotted corrugations, and full-length corrugations with 0.8 mm sheet thickness as the reference (Figure 2.15). The full scale UAS impacts were simulated and the full-length corrugations behaved the best as they crushed axially during impact while the other two demonstrated a combination of axial crushing and bending behavior. They were also iterated for sheet thickness of 0.7, 0.8, 0.9, and 1.0 mm. The UAS penetrated the target for 0.7 mm MT sheet thickness (no perforation of any components was observed), while for all other cases it didn't perforate or penetrate. The energies absorbed by 0.8, 0.9, and 1.0 mm thick MT during the impact were relatively similar: 654, 653, 660 J, respectively with reference to full-length corrugations. Full-length corrugations with 0.8 mm sheet thickness was the chosen MT design based on energy absorption, crushing behavior, and minimum weight addition to UAS. Detailed geometric dimensions for the MT are described in Figure 2.16.

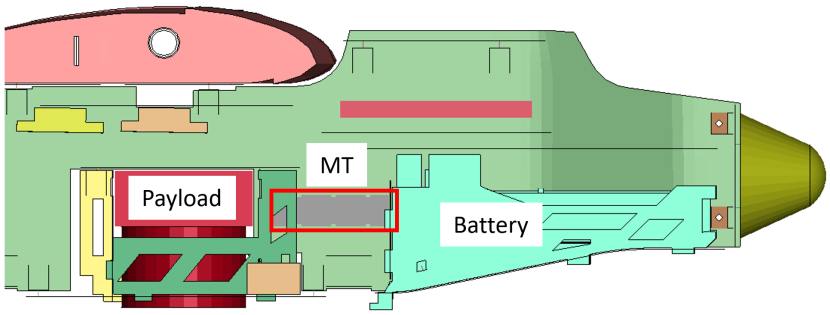

Figure 2.14: MT (in grey color) mounted between the payload front and battery aft PCBs.

Figure 2.15: MT cutout design iterations.

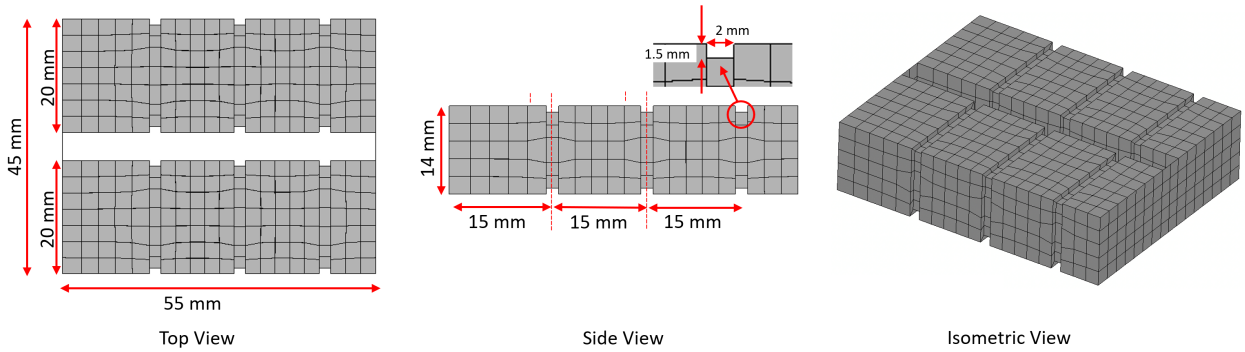

Figure 2.16: MT geometric design dimensions.

The MT were meshed using shell FEs with a nominal size of 3.5 mm, a maximum size of 4 mm, and a minimum size of 1.5 mm for corrugations. They were attached to payload front and battery aft PCBs (*cf.* Figure 2.14) through *CONTACT_TIED_NODES_TO_SURFACE*. *MAT_024 MAT_PIECEWISE_LINEAR_PLASTICITY* was the material model used for MT.

2.4.2 Design of Conical Metallic Nosecone (MNC)

Based on a similar idea as the MT, a hollow corrugated conical metallic nosecone (MNC) made of Al 6061-T6 was designed. Three full-length corrugations were used for MNC design with a sheet thickness of 0.8 mm. The nosecone had a diameter of 56 mm based on firewall dimensions and a length of 60 mm. A polymeric foam sleeve covered its surface to provide a smooth surface for aerodynamic considerations. The sleeve was made of IMPAXX700 foam and had a thickness of 6 mm. The detailed geometric design of MNC is shown in Figure 2.17.

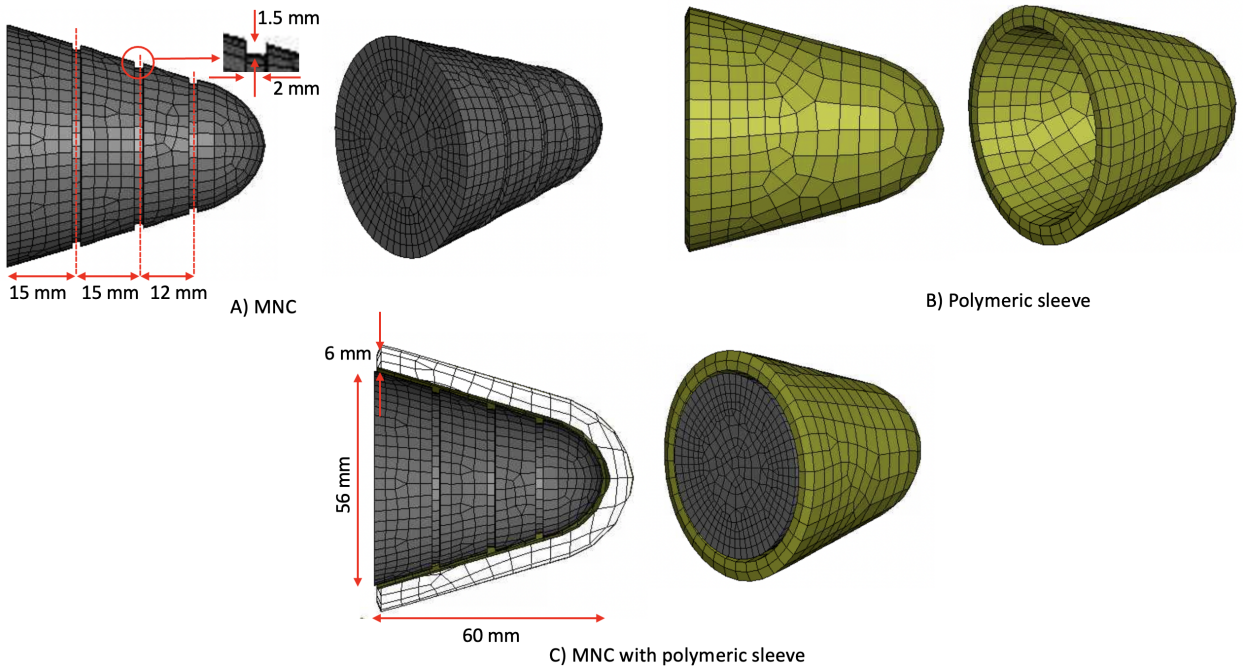

Figure 2.17: MNC and polymeric sleeve geometric designs.

The MNC was also modeled using shell FEs with a nominal size of 3.5 mm, a maximum size of

4 mm, and a minimum size of 1.5 mm. It was tied to the firewall through *NODAL_RIGID_BODIES*. The material model used for the MNC was the same as the MT. The polymeric sleeve and MNC had global *CONTACT_AUTOMATIC_SINGLE_SURFACE* between them. The sleeve was modeled using nominal 3.5 mm solid FEs. (MNC and polymeric sleeve co-exist and will be together referred to as MNC in the following sections).

2.4.3 UAS Impact Simulations with MT and MNC

UAS flat-plate impact simulations were performed with the MT and MNC individually and in combination: i) UAS with MT, ii) UAS with MNC, and iii) UAS with MT and MNC, using the baseline pusher configuration (Figure 2.18).

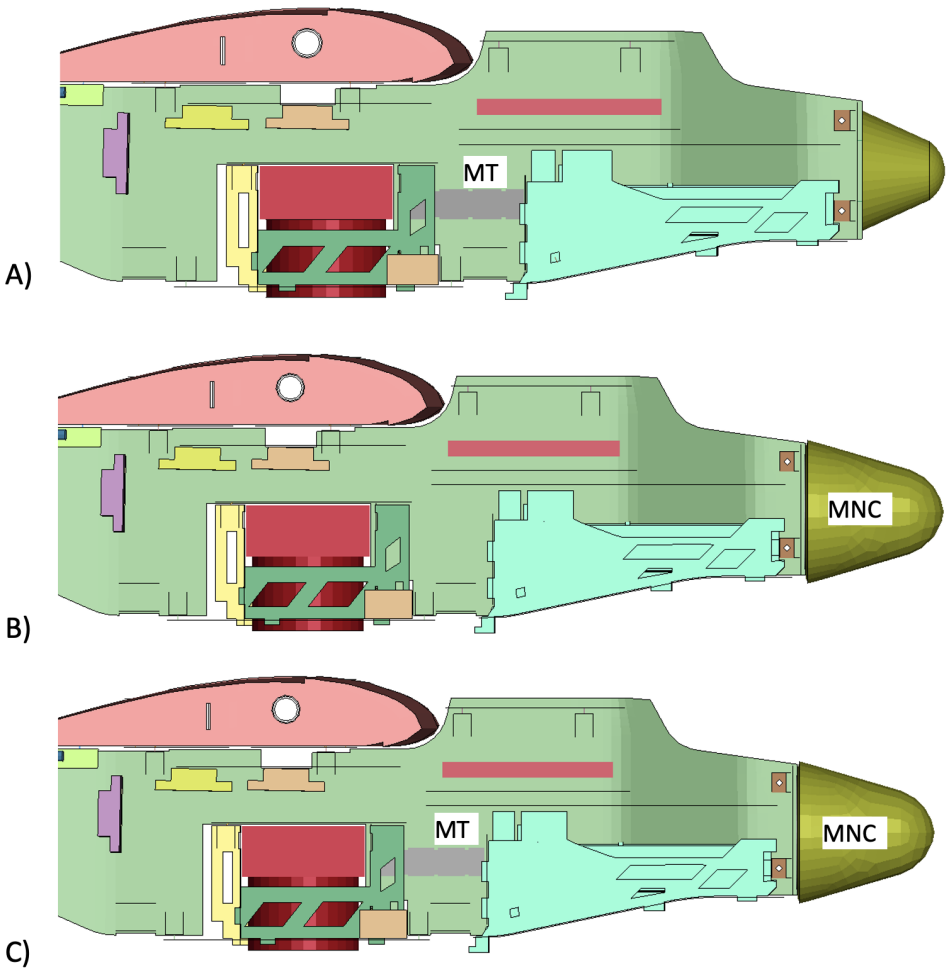

Figure 2.18: UAS with A) MT, B) MNC, and C) MT and MNC configurations.

All three configurations were successful in avoiding target plate tearing. These configurations were then evaluated based on the payload velocity at end of the simulated impact (t = 7 ms), strains experienced by the target plate in the impact region impact, and added weight due to the design changes. The strain evaluation region was selected around the first point of target impact covering 16X16 FEs around it. The select region was large enough to capture the primary impact of heavier components (battery, payload, and motor). Also, in all cases where the target plate tearing occurred, the plate tear originated in this region. The region is described in Figure 2.19. The comparison of payload impact velocity, target plate strains, and added weight among these configurations with metallic structures is presented in Table 2.4.

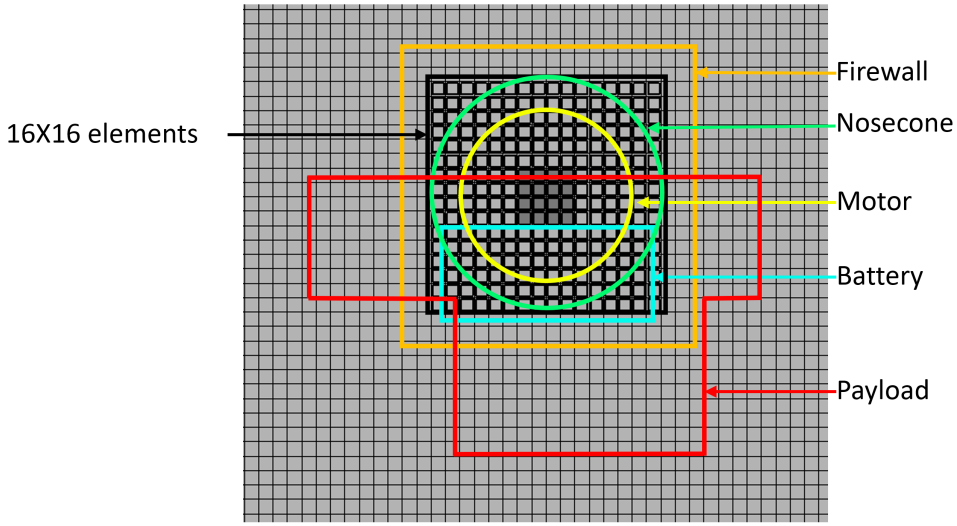

Figure 2.19: 16X16 target strain measurement elements highlighted in black along with schematic showing the heavier components' imprint over the strain measurement region.

Table 2.4: Frangibility efficiency comparison between UAS configurations with metallic structures.

UAS configuration	Payload velocity at 7 ms (m/s)	Target plate strain for		Added weight (g)
		Element max.	Avg max.	
MT	-24.9	0.123	0.0784	23.3 (1.3% of UAS)
MNC	-25.4	0.125	0.0817	26.9 (1.5% of UAS)
MT and MNC	-24.3	0.103	0.077	48.0 (2.6% of UAS)

The UAS configuration with MT and MNC was chosen as the final and optimal frangible design considering the payload velocity and target plate strains, and the added weight was also minimal. It was seen that the higher the negative payload velocity, the higher the target plate strains. This was the best design iteration for a non-penetrating frangible design. The global energies and energy ratio for this configuration were verified based on the LS-DYNA Aerospace Working Group (AWG) guidelines [54] (Figure 2.20). These guidelines state that the energy ratio should not vary beyond 0.99-1.01 along with the hourglass energy being less than 10% of the peak internal energy to limit the spurious zero-energy modes arising due to under-integrated element formulations. The initial setup at t = 0 ms and the impact kinematics at t = 7 ms for this configuration are shown in Figure 2.21.

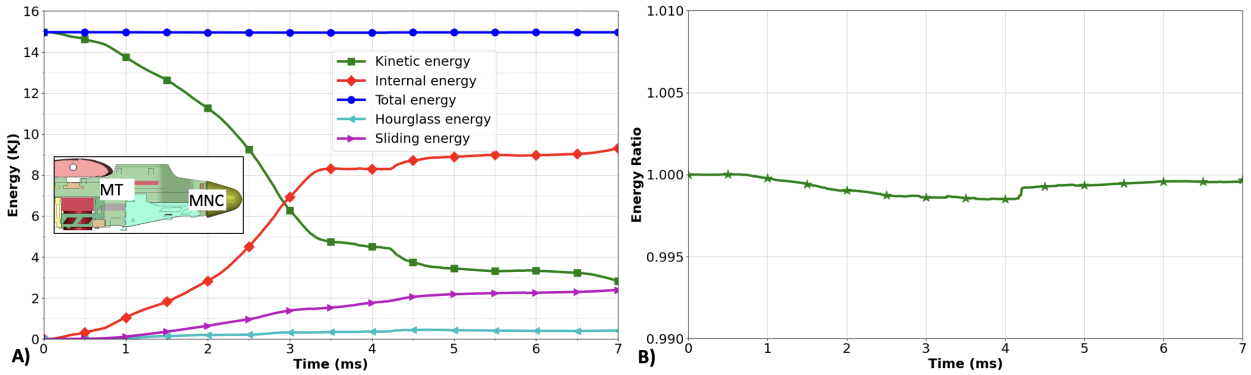

Figure 2.20: A) Global energies and B) energy ratio for frangible UAS design with MT and MNC against the deformable flat-plate target.

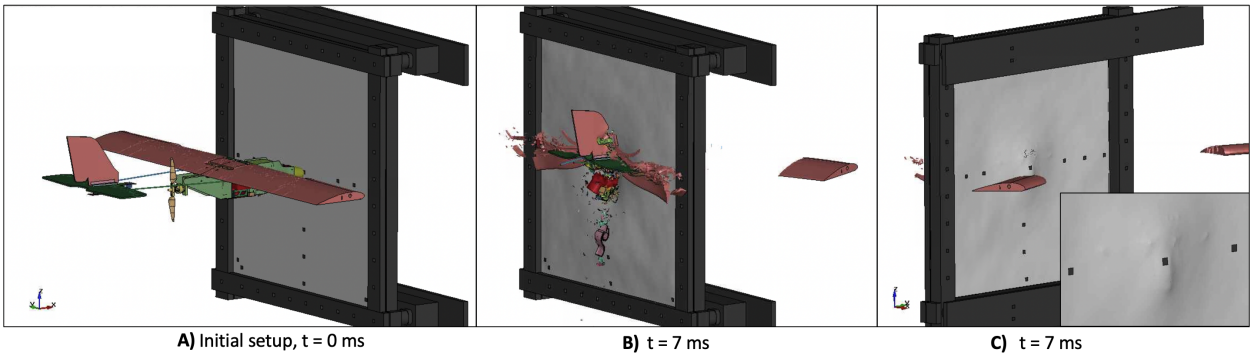

Figure 2.21: Frangible UAS with MT and MNC: A) impact side initial setup at $t = 0$ ms B) impact side final kinematics at $t = 7$ ms C) exit side final kinematics at $t = 7$ ms and zoomed view of the center of the target in inset.

Comparing optimal frangible design results with the tractor configuration where the target was perforated instantly, no tearing was observed for the frangible pusher design. In this case, the target plate had a maximum strain of 10.3% compared to the plate failure strain of 16.8% (computed from the failed elements in the case where target plate tearing occurred) which gives a 39% safety margin. A comparison of payload impact velocity for frangible design iterations progressing towards the optimal frangible design from tractor configuration is presented in Figure 2.22. For the tractor UAS, the payload perforates through the target very early ($t = \sim 2.75$ ms) retaining most of its velocity. For all the pusher configuration frangible designs, a decline in the payload velocity is observed during the initial stages of the impact. This is due to the cushioning of the payload impact by the battery which fragments upon impacting the target. As the payload moves forward, it slows down to its minimum velocity (the dip between $t = 4$ and 5 ms) due to the resistance from the target and in the process tears the target. After this, the payload velocity increases (the rise after the '*') due to the motor impact on it, pushing it through the target and then achieves a constant velocity. However, looking at the UAS design with MT and MNC, the payload velocity goes negative and stays negative throughout the impact duration manifesting that the payload, and hence, the UAS did not perforate the target. This shows that such designs will be successful in reducing the damage severity in airborne collisions against manned aircraft.

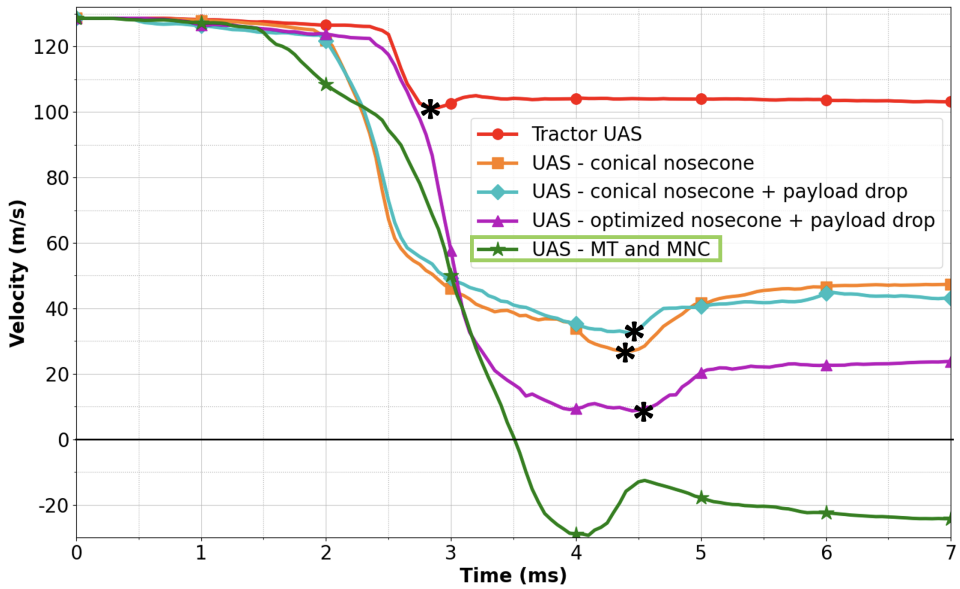

Figure 2.22: Payload impact velocity comparison. ('*' represents the instant when the payload perforates through the target).

2.5 Frangible UAS FE Model Stability Verification for Future Air-to-Air Collisions Simulations

The UAS configuration with MT and MNC was used as the final frangible design to simulate air-to-air collisions with commercial and business jet aircraft. Worst case tractor UAS collision scenarios were identified from [16, 19]. These worst case collision scenarios (highest severity index *i.e.*, level IV: maximum damage to the target) are being simulated with frangible UAS to evaluate the effectiveness of the frangible design in damage severity reduction in realistic scenarios. This work is being performed in collaboration with the NIAR. It was predicted in [16, 19] that in certain cases, tractor UAS impacts against commercial and business jet aircraft resulted in perforation of the aircraft skin and the UAS impacted the underlying, relatively rigid, load carrying structures (identified as level IV severity) such as ribs and spars at different angles and orientations. These impact conditions influence the FE model numerical stability and robustness. Thus, the frangible UAS model was verified for numerical stability and robustness before performing air-to-air collisions through rigid flat-plate and rigid knife-edge target impacts.

2.5.1 Frangible UAS Impacts Against Rigid Flat-Plate Target

Compliant projectile impacts against a rigid target may result in numerical instabilities in the FE model due to excessive localized deformation. As the frangible UAS design can encounter these (rigid target impact) scenarios in air-to-air collisions with the commercial and business jet aircraft, such stability verification of the FE model was necessary. The rigid target impact was simulated by modifying the deformable flat-plate target to a rigid flat-plate target using LS-DYNA *DEFORMABLE_TO_RIGID* card. The impact was simulated at 128.6 m/s and the global energies and energy ratio plots (Figure 2.23) were assessed for stability which indicated that the simulations were numerically stable and robust as per LS-DYNA AWG modeling guidelines [54]. These guidelines state that the energy ratio should not vary beyond 0.99-1.01 along with the hourglass energy being less than 10% of the peak internal energy to limit the spurious zero-energy modes arising due to under-integrated element formulations.

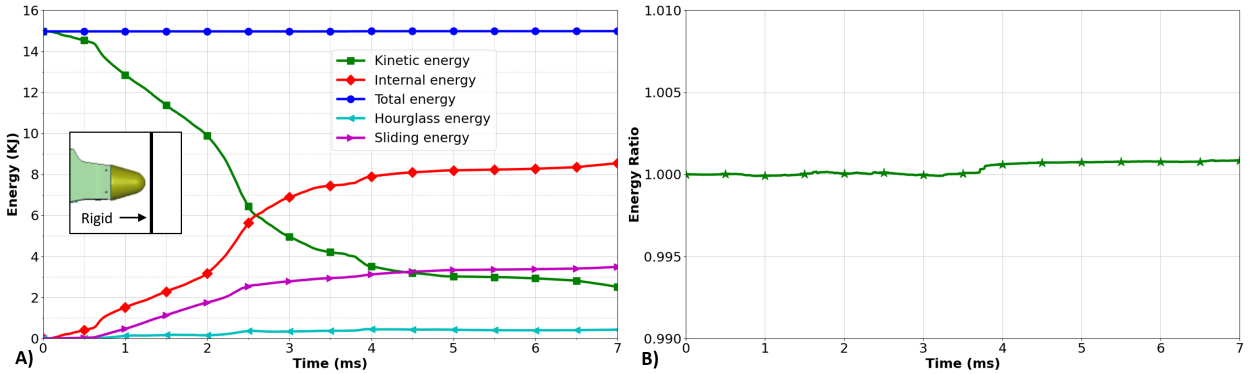

Figure 2.23: A) Global energies and B) energy ratio for frangible UAS impact against rigid flat-plate target.

2.5.2 Frangible UAS Impacts Against Rigid Knife-Edge Target

Similar to flat rigid-target impacts, compliant projectile impacts to rigid knife-edge targets can also result in numerical instability and this case was also verified for the frangible UAS FE model. Knife-edge impacts were setup by modeling a rigid target plate using LS-DYNA *MAT_20*

MAT_RIGID material card with the plate edge facing the UAS (Figure 2.24). The knife-edge impact location was selected such that all the new components introduced into the UAS strike the knife, the tractor configuration had already been validated for rigid knife-edge impacts [19]. The impact simulation was performed at 128.6 m/s and the global energies and energy ratio plots (Figure 2.25) were assessed for the stability of the simulations which indicated that the simulation was numerically stable and robust as per LS-DYNA AWG guidelines [54] (described previously).

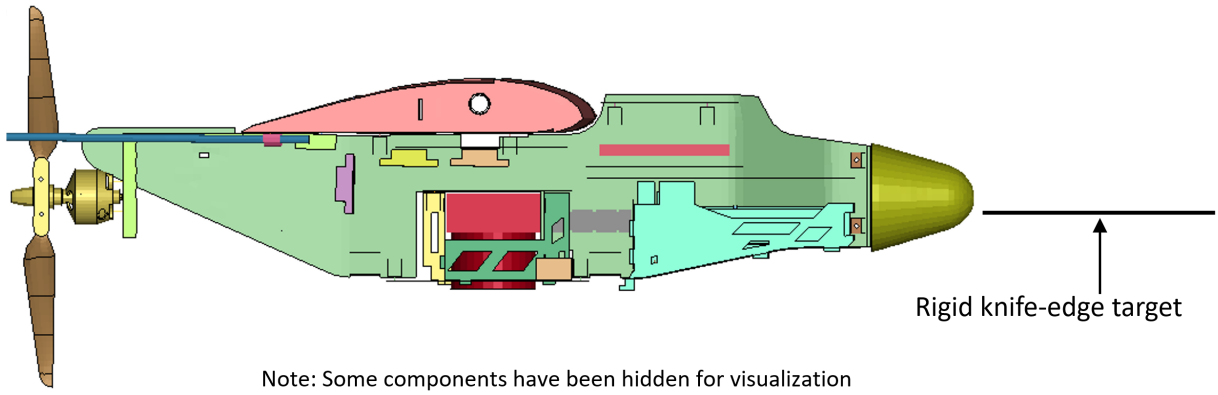

Figure 2.24: Frangible UAS FE model setup for rigid knife-edge impact.

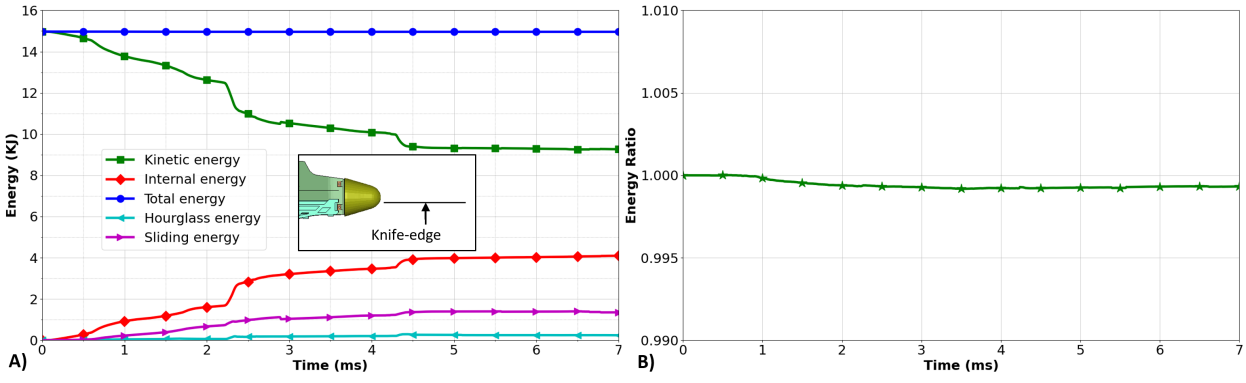

Figure 2.25: A) Global energies and B) energy ratio for frangible UAS impact against rigid knife-edge target.

The frangible UAS FE model proved to be numerically stable and robust for all the target scenarios (deformable flat-plate, rigid flat-plate, and rigid knife-edge) that it can encounter in an air-to-air collision. The model was then provided to the NIAR for performing air-to-air collision simulations with commercial and business jet aircraft to evaluate the effectiveness of the frangible design in realistic scenarios.

2.6 Conclusions

Frangible design concepts to mitigate fixed-wing UAS's collision damage to targets were explored through a baseline pusher engine UAS configuration by simulating impacts against a flat-plate Al target. The frangible UAS designs with i) polymeric nosecone, ii) payload drop mechanism, and iii) optimized nosecone with payload drop mechanism reduced the impact damage severity compared to tractor UAS configuration. They progressively lowered the payload velocity after target perforation by 54%, 59%, and 78%, respectively compared to tractor UAS impacts. However, they could not eliminate target plate tearing and perforation. The payload drop mechanism and polymeric foams were not efficient in target damage reduction for such high velocity UAS (128.6 m/s) impacts. For polymeric foams, there is a weight and volume penalty for increasing the energy absorption which is not always feasible. For the payload drop mechanism, the high impact velocity does not give it enough time to drop substantially but it may be advantageous in low velocity impacts. The UAS configuration with metallic structures (MT and MNC) successfully avoided target plate tearing and provided a 39% safety margin based on target plate strain to failure with minimal weight addition (2.6%). The energy absorbing metallic corrugated tubes and the metallic corrugated nosecone were efficient in impact energy absorption and could be adapted into other pusher configuration fixed-wing UASs with similar structure and components to mitigate impact damage at such high velocities. These frangible designs will reduce the impact damage to manned aircraft in air-to-air collision scenarios and ensure safer airspace.

2.7 Future Work

The frangible UAS design with metallic corrugated tubes (MT) and a metallic corrugated nosecone (MNC) will be used to simulate worst case collision scenarios against commercial and business jet aircraft as identified from [16, 19]. This will be done to evaluate the effectiveness of frangible design in mitigating collision damage in real scenarios. The work will be done in collaboration with the NIAR as they have the full scale FE models of the commercial and business jet aircraft.

There is also scope for improvement in the design of the metallic corrugated tubes and nosecone. They can be optimized for sheet thickness, overall length, number of corrugations, spacing between corrugations, depth, and shape of corrugations, orientation *etc.* for improving their energy absorption capacity and minimizing the peak target strains to further reduce impact damage. This can result in even lighter energy absorption structures for UAS and those design recommendations can be extended to other fixed-wing UASs to mitigate the impact damage. The UAS mass can be scaled to replicate higher mass small UASs to see the effectiveness of these frangible design concepts in those scenarios which will provide guidance for developing frangible designs for higher mass small UASs.

3. ONGOING AND FUTURE WORK

3.1 Ongoing and Future Work

The fixed-wing UAS pusher configuration with metallic corrugated tubes (MT) and a metallic nosecone (MNC) was chosen as the optimal frangible design for simulating the air-to-air collision impacts against commercial and business jet aircraft, after verifying FE model stability for rigid flat-plate and rigid knife-edge targets. Worst case collision scenarios for the tractor UAS impacts against commercial and business jet aircraft primary structures were identified from [16, 19]. The aircraft primary structures involved horizontal and vertical stabilizers, wing leading edge, and windshield. The UAS impacts were simulated at multiple locations on these primary structures and were categorized into different severity levels ranging from I-IV [16, 19] based on the target damage. Level IV was the highest level of damage severity where the UAS perforated aircraft skin and impacted underlying structures (worst case scenario). These worst case scenarios, a total of seven, shown in Figure 3.1, were chosen to be simulated with the frangible UAS design to evaluate its effectiveness. This work is being performed in collaboration with the NIAR. The frangible UAS will reduce the damage severity for air-to-air collision scenarios with manned aircraft which has been highlighted by the preliminary simulations done at the NIAR. These results will be presented in a future work.

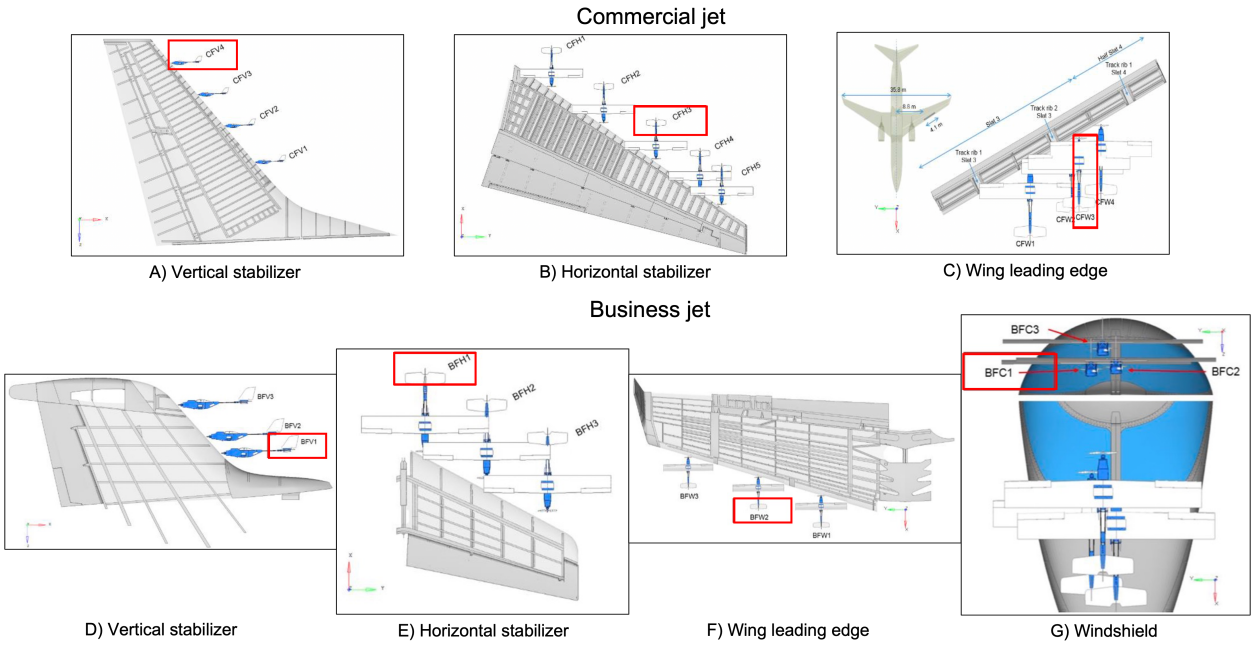

Figure 3.1: Fixed-wing UAS impacts simulated against commercial and business jet aircraft primary structures, worst case scenarios highlighted in red boxes (adapted from [16]).

3.2 Modifications to Frangible UAS FE Model for Integration into Full Scale Airborne Collision Simulations

Prior to simulating the frangible UAS impacts against commercial and business jet aircraft with the NIAR, the simulated UAS impact to flat-plate was used for benchmarking the FE predictions between the Texas A&M University (TAMU) and the NIAR. The frangible UAS impacts to flat-plate were simulated in LS-DYNA version R12.1.0, however, the NIAR commercial and business jet models were validated in R10.2.0. While benchmarking, it was observed that the different LS-DYNA versions yielded different results, particularly in the tearing of the flat-plate, and sliding and hourglassing energy predictions. Also, the friction coefficients in global contact algorithms had a significant effect on the predictions across different LS-DYNA versions. These differences were likely due to updates in the contact algorithms and features implemented for enhancing stability and robustness in LS-DYNA R12.1.0. The specific details for contact algorithms and solver updates for these LS-DYNA versions can be found in their manuals [55, 56]. Certain LS-DYNA contact

and control parameters were fine-tuned to achieve similar predictions across the two LS-DYNA versions. The final fixed-UAS model had an independent *ERODING_SINGLE_SURFACE* contact for the battery. The global contacts had coefficients of static and dynamic friction as 0.3 and 0.3. All non-metallic shell FEs in the UAS FE model were added to *NFAIL* in *CONTROL_SHELL* and all the solid FEs to *PSFAIL* in *CONTROL_SOLID*. This final model did not tear the target and showed a good correlation between the TAMU and the NIAR, verified using effective plastic strain in the target with less than 3% variation between the two. The frangible UAS FE model developed as part of this thesis will be capable of reducing the damage severity upon impact to manned aircraft.

3.3 Lessons Learnt

From this thesis, it can be learned that the pusher configuration UAS impacts are less severe than the tractor configuration impacts. Simple structural changes to the UAS design can significantly reduce the UAS collision damage to targets with minimal weight addition. Comparing the energy absorbing mechanisms, polymeric foams being less stiff and having lower elastic limits are not suitable for very high velocity (128.6 m/s) or high energy impacts. They incur weight and volume penalties which is not always feasible to incorporate into the system and can pose additional challenges like thermal cooling of auxiliary systems, mounting constraints *etc.* They can find applications in low velocity/energy impacts and curved or complex geometries. The payload drop mechanism is also not advantageous at such high velocity impacts as it does not give enough time for the payload to drop substantially. But it may be advantageous for low velocity and high energy impacts where a significant momentum can be lost from the total momentum of the system. The metallic structures can absorb a large amount of energy due to their high stiffness and large elastic limits. Unique geometric designs can be implemented to ensure minimal weight for metallic structures. Crushing and buckling modes are enabled for energy absorption by metallic structures to limit the peak impact forces as they can be very stiff. Appropriate designs of metallic structures can be very successful in mitigating damage for high velocity, high energy impacts.

REFERENCES

[1] D. Jenkins and B. Vasigh, *The economic impact of unmanned aircraft systems integration in the united states*. Association for Unmanned Vehicle Systems International (AUVSI), 2013.

[2] Federal Aviation Administration, "FAA aerospace forecast: fiscal years 2019-2039." https://www.faa.gov/data_research/aviation/aerospace_forecasts/media/FY2019-39_FAA_Aerospace_Forecast.pdf. Accessed: 2022-08.

[3] Federal Aviation Administration, "FAA advisory circular 107-2." https://www.faa.gov/documentlibrary/media/advisory_circular/ac_107-2.pdf. Accessed: 2022-08.

[4] Federal Aviation Administration, "UAS sightings report." https://www.faa.gov/uas/resources/public_records/uas_sightings_report/. Accessed: 2022-08.

[5] Federal Aviation Administration, "FAA releases updated drone sighting reports." https://www.faa.gov/newsroom/faa-releases-updated-drone-sighting-reports?newsId=87565. Accessed: 2022-08.

[6] Safety and Health, "For airplanes, drone collisions a greater hazard than bird strikes: FAA study." https://www.safetyandhealthmagazine.com/articles/16546-for-airplanes-drone-collisions-a-greater-hazard-than-bird-strikes-faa-study. Accessed: 2022-08.

[7] CBS Broadcasting Inc., "Drone hits army helicopter flying over Staten Island." https://www.cbsnews.com/newyork/news/drone-hits-army-helicopter/. Accessed: 2022-08.

[8] BBC News Services, "Drone collides with commercial aeroplane in Canada." https://www.bbc.com/news/technology-41635518. Accessed: 2022-08.

[9] The Guardian, "Drone hits plane at Heathrow airport, says pilot." https://www.theguardian.com/uk-news/2016/apr/17/drone-plane-heathrow-airport-british-airways. Accessed: 2022-08.

[10] Wikipedia, "List of UAV-related incidents." https://en.wikipedia.org/wiki/List_of_UAV-related_incidents. Accessed: 2022-08.

[11] Authority, British Military Aviation, "Small remotely piloted aircraft systems (drones)-mid-air collision study," *Report-16*, pp. 9–16, 2016.

[12] H. Liu, H. C. M. Mohd, B. F. Ng, and K. H. Low, "Airborne collision evaluation between drone and aircraft engine: effects of position and posture on damage of fan blades," *AIAA Aviation 2020 Forum*, p. 3214, 2020. doi: https://doi.org/10.2514/6.2020-3214.

[13] X. Meng, Y. Sun, J. Yu, Z. Tang, J. Liu, T. Suo, and Y. Li, "Dynamic response of the horizontal stabilizer during uas airborne collision," *International Journal of Impact Engineering*, vol. 126, pp. 50–61, 2019. doi: https://doi.org/10.1016/j.ijimpeng.2018.11.015.

[14] T. Lyons and K. D'Souza, "Parametric study of a unmanned aerial vehicle ingestion into a business jet size fan assembly model," *Journal of Engineering for Gas Turbines and Power*, vol. 141, 01 2019. doi: https://doi.org/10.1115/1.4042286.

[15] G. Olivares, L. Gomez, J. Espinosa de los Monteros, R. J. Baldridge, C. Zinzuwadia, and T. Aldag, "Volume II-UAS airborne collision severity evaluation-quadcopter," 2017. https://trid.trb.org/view/1490822.

[16] G. Olivares, T. E. Lacy, L. Gomez, J. Espinosa de los Monteros, R. J. Baldridge, C. Zinzuwadia, T. Aldag, K. R. Kota, T. Ricks, and N. Jayakodi, "Volume III–UAS airborne collision severity evaluation–fixed-wing," 2017. https://trid.trb.org/view/1490823.

[17] K. D'Souza, T. Lyons, T. E. Lacy, and K. R. Kota, "Volume IV-UAS airborne collision severity evaluation-engine ingestion," 2017. https://trid.trb.org/View/1490824.

[18] X. Lu, X. Liu, Y. Li, Y. Zhang, and H. Zuo, "Simulations of airborne collisions between drones and an aircraft windshield," *Aerospace Science and Technology*, vol. 98, p. 105713, 2020. doi: https://doi.org/10.1016/j.ast.2020.105713.

[19] K. R. Kota, *Development and verification of a finite element model of a fixed-wing unmanned aerial system for airborne collision severity evaluation*. PhD thesis, Mississippi State University, 2018.

[20] K. R. Kota, T. Ricks, L. Gomez, J. Espinosa de los Monteros, G. Olivares, and T. E. Lacy, "Development and validation of finite element impact models of high-density UAS components for use in air-to-air collision simulations," *Mechanics of Advanced Materials and Structures*, vol. 27, no. 13, pp. 1178–1199, 2020. doi: https://doi.org/10.1080/15376494.2020.1740956.

[21] Y. S. Lee, N. H. Park, and H. S. Yoon, "Dynamic mechanical characteristics of expanded polypropylene foams," *Journal of Cellular Plastics*, vol. 46, no. 1, pp. 43–55, 2010. doi: https://doi.org/10.1177/0021955X09346363.

[22] D. D. Vries, "Characterization of polymeric foams." https://www.mate.tue.nl/mate/pdfs/10702_sec.pdf, 2009. Accessed: 2022-08.

[23] Anurag, K. R. Kota, and T. E. Lacy, "Development of a frangible design of small fixed-wing unmanned aerial system," in *Proceedings of the American Society for Composites - 36th Technical Conference*, 09 2021. doi: https://doi.org/10.12783/asc36/35750.

[24] G. Olivares, "FAA sUAS COE task A3 UAS airborne collision hazard severity evaluation." https://www.researchgate.net/publication/330764346_FAA_sUAS_COE_Task_A3_UAS_Airborne_Collision_Hazard_Severity_Evaluation, 11 2017. doi: 110.13140/RG.2.2.30840.08968.

[25] D. S. Cairns, G. Johnson, M. Edens, and F. Arnold, "Volume I-UAS airborne collision severity evaluation-projectile and target definition," 2016.

[26] Federal Aviation Administration, "Integration of civil unamanned aircraft systems (UAS) in the National Airspace System (NAS) roadmap." https://www.faa.gov/uas/resources/policy_library/media/Second_Edition_Integration_of_Civil_UAS_NAS_Roadmap_July%202018.pdf, 2018. Accessed: 2022-08.

[27] Y. Song, B. Horton, and J. Bayandor, "Investigation of UAS ingestion into high-bypass engines, Part 1: bird vs. drone," *58th AIAA/ASCE/AHS/ASC Structures, Structural Dynamics, and Materials Conference*, 2017. doi: https://doi.org/10.2514/6.2017-0186.

[28] K. Schroeder, Y. Song, B. Horton, and J. Bayandor, "Investigation of UAS ingestion into high-bypass engines, Part 2: parametric drone study," *58th AIAA/ASCE/AHS/ASC Structures, Structural Dynamics, and Materials Conference*, 2017. doi: https://doi.org/10.2514/6.2017-0187.

[29] Federal Aviation Administration, "14 CFR § 25-Airworthiness standards: Transport category airplanes (Section 25.631: Bird strike damage)." https://www.law.cornell.edu/cfr/text/14/25.631. Accessed: 2022-08.

[30] Federal Aviation Administration, "14 CFR § 25-Airworthiness standards: Transport category airplanes (Section 25.571: Damage-tolerance and fatigue evaluation of structure)." https://www.law.cornell.edu/cfr/text/14/25.571. Accessed: 2022-08.

[31] Federal Aviation Administration, "14 CFR § 35.36-Airworthiness standards: Propellors (Section 35.36: Bird impact)." https://www.law.cornell.edu/cfr/text/14/35.36. Accessed: 2022-08.

[32] J. L. Deaton, *Investigating collision avoidance for small UAS using cooperative surveillance and ACAS X*. PhD thesis, Massachusetts Institute of Technology, 2019.

[33] Virtual Expo Group - Direct Industry, "Fixed-wing UAV VAMP." https://www.directindustry.com/prod/bormatec/product-100937-936071.html. Accessed: 2022-08.

[34] Virtual Expo Group - Aero Expo, "Industrial drone CAM-FLYERG." https://www.aeroexpo.online/prod/bormatec/product-171269-11135.html. Accessed: 2022-08.

[35] Virtual Expo Group - Direct Industry, "Fixed-wing UAV MAJA." https://www.directindustry.com/prod/bormatec/product-100937-936043.html. Accessed: 2022-08.

[36] Virtual Expo Group - Aero Expo, "Industrial drone EXPLORER." https://www.aeroexpo.online/prod/bormatec/product-171269-11152.html. Accessed: 2022-08.

[37] Virtual Expo Group - Aero Expo, "Professional UAV Tango2." https://www.aeroexpo.online/prod/draganfly-drones/product-175762-26428.html. Accessed: 2022-08.

[38] B. Croop and H. Lobo, "Selecting material models for the simulation of foams in ls-dyna," *7th European LS-Dyna Conference*, pp. 1–6, 2009.

[39] S. R. Muthyala, *Improvement in crashworthiness of a vehicle for side impact occupant protection using IMPAXX and polyurethane high energy-absorbing foam materials*. Master's thesis, Wichita State University, 2017.

[40] G. Slik, G. Vogel, and V. Chawda, "Material model validation of a high efficient energy absorbing foam," in *Proceedings of the 5th LS-DYNA Forum*, 2006.

[41] MatWeb Material Property Data, "Aluminum 7075-T6; 7075-T651." http://www.matweb.com/search/DataSheet.aspx?MatGUID=4f19a42be94546b686bbf43f79c51b7d&ckck=1. Accessed: 2022-08.

[42] Livermore Software Technology Corporation (LSTC), Livermore, CA., "LS-TaSC™ Theory Manual, Version 4.1," 2019.

[43] Rozvany, G.I.N, *Structural Design via optimality criteria*. Kluver Academic Publishers, 1989.

[44] MP Bendsoe and O Sigmund, *Topology optimization: Theory, methods and applications*. Springer, 2003.

[45] G. I. N. Rozvany, "Topology optimization in structural mechanics," 1997. doi: https://doi.org/10.1007/978-3-7091-2566-3.

[46] H. A. Eschenauer and N. Olhoff, "Topology optimization of continuum structures: A review," *Applied Mechanics Reviews*, vol. 54, pp. 331–390, 07 2001. doi: https://doi.org/10.1115/1.1388075.

[47] A. Tovar, *Bone remodeling as a hybrid cellular automaton optimization process*. PhD thesis, University of Notre Dame, 2004.

[48] N. Patel, *Crashworthiness design using topology optimization*. PhD thesis, University of Notre Dame, 2007.

[49] Livermore Software Technology Corporation (LSTC), Livermore, CA., "LS-TaSC™ User's Manual, Version 4," 2019.

[50] L. M. M. Boermans, "Research on sailplane aerodynamics at delft university of technology," *Technical Soaring*, vol. 30, pp. 10–12, 2006.

[51] R. R. Sahu and P. K. Gupta, "Improvement of crush can configuration," *International Journal of Crashworthiness*, vol. 19, no. 6, pp. 600–612, 2014. doi: https://doi.org/10.1080/13588265.2014.929375.

[52] S. C. K. Yuen and G. N. Nurick, "The energy-absorbing characteristics of tubular structures with geometric and material modifications: An overview," *Applied Mechanics Reviews*, vol. 61, 03 2008. doi: https://doi.org/10.1115/1.2885138.

[53] C. Zhou, S. Ming, C. Xia, B. Wang, X. Bi, P. Hao, and M. Ren, "The energy absorption of rectangular and slotted windowed tubes under axial crushing," *International Journal of Mechanical Sciences*, vol. 141, pp. 89–100, 2018. doi: https://doi.org/10.1016/j.ijmecsci.2018.03.036.

[54] LS-DYNA Aerospace Working Group, "Modeling Guidelines Document." https://awg.lstc.com/tiki-index.php?page=Resources. Accessed: 2022-08.

[55] Livermore Software Technology Corporation (LSTC), Livermore, CA., "LS-DYNA Keyword User's Manual, Volume I, R10.0," 2017.

[56] Livermore Software Technology Corporation (LSTC), Livermore, CA., "LS-DYNA Keyword User's Manual, Volume I, R12.0," 2020.